

A *ROSAT* HRI survey of bright nearby galaxies

T. P. Roberts and R. S. Warwick

Department of Physics and Astronomy, University of Leicester, University Road, Leicester, LE1 7RH

ABSTRACT

We use the extensive public archive of *ROSAT* High Resolution Imager (HRI) observations to carry out a statistical investigation of the X-ray properties of nearby galaxies. Specifically we focus on the sample of 486 bright ($B_T \leq 12.5$) northern galaxies studied by Ho, Filippenko and Sargent (HFS) in the context of their exploration of the optical spectroscopic properties of nearby galactic nuclei. Over 20% of HFS galaxies are encompassed in *ROSAT* HRI fields of reasonable (≥ 10 ks) exposure. The X-ray sources detected within the optical extent of each galaxy are categorised as either nuclear or non-nuclear depending on whether the source is positioned within or outside of a $25''$ radius circle centred on the optical nucleus.

A nuclear X-ray source is detected in over 70% of the galaxies harbouring either a Seyfert or LINER nucleus compared to a detection rate of only $\sim 40\%$ in less active systems. The correlation of the $H\alpha$ luminosity with nuclear X-ray luminosity previously observed in QSOs and bright Seyfert 1 galaxies appears to extend down into the regime of ultra-low luminosity ($L_X \sim 10^{38} - 10^{40}$ erg s^{-1}) active galactic nuclei (AGN). The inferred accretion rates for this sample of low-luminosity AGN are significantly sub-Eddington.

In total 142 non-nuclear sources were detected. In combination with published data for M31 this leads to a luminosity distribution (normalised to an optical blue luminosity of $10^{10} L_\odot$) for the discrete X-ray source population in spiral galaxies of the form $dN/dL_{38} = (1.0 \pm 0.2)L_{38}^{-1.8}$, where L_{38} is the X-ray luminosity in units of 10^{38} erg s^{-1} . The implied L_X/L_B ratio is $\sim 1.1 \times 10^{39}$ erg $s^{-1} (10^{10} L_\odot)^{-1}$. The nature of the substantial number of “super-luminous” non-nuclear objects detected in the survey is discussed.

Key words: galaxies:general - galaxies:active - X-rays:galaxies

1 INTRODUCTION

The *ROSAT* public archive now includes over 4400 pointed observations carried out with the *ROSAT* High Resolution Imager (HRI) during the period June 1990 to December 1997. One obvious application of this extensive database is the investigation of the X-ray properties of particular classes of object, especially those which are available in large numbers as the result of detailed surveys carried out in other wavebands. This is the approach adopted in the present paper which focuses on the luminous discrete X-ray sources associated with nearby bright galaxies.

For this purpose we use the sample of 486 bright ($B_T \leq 12.5$) predominantly northern ($\delta > 0^\circ$) galaxies studied by Ho, Filippenko & Sargent (1995) in the context of their search for “dwarf” Seyfert nuclei in nearby galaxies. It turns out that, of the galaxies studied by Ho, Filippenko and Sargent (hereafter the HFS sample), over 20% lie within the field of view of reasonably deep (≥ 10 ks exposure) *ROSAT* HRI observations. As part of their programme

Ho, Filippenko & Sargent (1995, 1997a,b,c) have compiled a huge database of information pertaining to both the optical spectroscopic properties of the galaxy nuclei and the properties of the host galaxy. This comprehensive and coherent body of information provides an ideal resource for our present purpose.

The first detailed studies of the X-ray properties of nearby galaxies utilised the X-ray imaging and spectroscopic capabilities of the *EINSTEIN* Observatory (as summarised in the *EINSTEIN* results atlas published by Fabbiano, Kim & Trinchieri 1992 and more recently in the work of Burstein et al. 1997). The Einstein observations demonstrated that the X-ray emission from bright elliptical and lenticular galaxies is often dominated by their hot interstellar medium, whereas in normal spirals it is the integrated emission of evolved stellar sources, such as supernova remnants (SNRs) and X-ray binaries (XRBs) which is generally most important (see Fabbiano 1989 for a review). *EINSTEIN* studies also established that, barring the presence of

arXiv:astro-ph/0001209v1 12 Jan 2000

a luminous active galactic nucleus (AGN), the X-ray luminosity exhibited by normal galaxies is typically in the range $10^{38} - 10^{42}$ erg s $^{-1}$. *ROSAT* observations have now added considerably to this picture. Specifically the high sensitivity, soft bandpass, modest spectral resolution and $< 30''$ spatial resolution of the *ROSAT* X-ray telescope/position sensitive proportional counter (PSPC) combination has greatly extended our knowledge of diffuse $10^6 - 10^7$ K thermal emission in galaxies and has confirmed the ubiquity of such emission not only in early type and starburst galaxies but also as a significant component in normal spirals (e.g. Read, Ponman & Strickland 1997). Both *ROSAT* PSPC and HRI observations have also furthered our knowledge of the resolved point X-ray source population in nearby galaxies, for example with the detection of hundreds of such sources in M31 (Primini et al. 1993; Supper et al. 1997).

Although the *ROSAT* PSPC provided somewhat more sensitivity than the *ROSAT* HRI, the advantage of using data from the latter instrument is that, by and large, it is possible to focus the investigation on a single theme, namely the resolved discrete X-ray sources associated with nearby galaxies. Moreover the high spatial resolution afforded by the *ROSAT* HRI (FWHM $< 10''$) is particularly relevant when attempting to distinguish the emission of putative low-luminosity AGN from other luminous source populations in galaxies. The remainder of this paper is ordered as follows. In section 2 we describe the available database of HRI observations, the possible impact of selection effects in the X-ray data and the method used to detect point X-ray sources in each HRI field. Next, in section 3, we carry out a preliminary analysis of the X-ray source sample, distinguishing between the “nuclear” and “non-nuclear” source populations. We also estimate the likely level of contamination by foreground stars and background QSOs. Section 4 then investigates the incidence of luminous nuclear X-ray sources in galaxies with nuclei of different optical spectroscopic type. Section 5 goes on to consider the X-ray luminosity distribution of the non-nuclear source population and the nature of the substantial subset of “super-luminous” sources. Finally in section 6 we provide a brief summary of our findings.

2 THE X-RAY DATABASE

The relevant subset of *ROSAT* HRI pointed observations was identified by cross-correlating the ROSPUBLIC database (circa July 1998) available from the Leicester Data Archive Service (LEDAS) with the full list of HFS galaxy (*i.e.* optical nuclear) positions. All HRI fields which encompassed the HFS galaxy position within $15'$ of the pointing position and had an exposure of at least 10 ks were initially accepted. This process led to a set of 148 HRI observations of 106 HFS galaxies (with many of the galaxies having been observed more than once). However, a number of these observations were unsuitable for our purposes. The two dominant Local Group members, NGC 224 (M 31) and NGC 598 (M 33), were not included as their full angular extent cannot be imaged in a single HRI observation. The HRI observations of NGC 1275 and NGC 4478/4486 were not used since these galaxies lie at the centre of galaxy clusters (Perseus and Virgo respectively) and the presence of a bright intra-cluster medium confuses the X-ray field and limits the

point source sensitivity. Similarly to avoid the complication of the dominant hot interstellar medium in massive early type galaxies, ellipticals and lenticulars with $M_B < -20.5$ were excluded, as was the bright starburst galaxy NGC 3034 (M82). Finally the galaxies NGC 1052 and 4594 were rejected as southern interlopers in the HFS sample. A total of 83 galaxies remained, covered by 111 HRI observations, representing roughly a 17% sampling of the full HFS catalogue. Hereafter we refer to our HRI-observed subset of HFS galaxies as the XHFS sample.

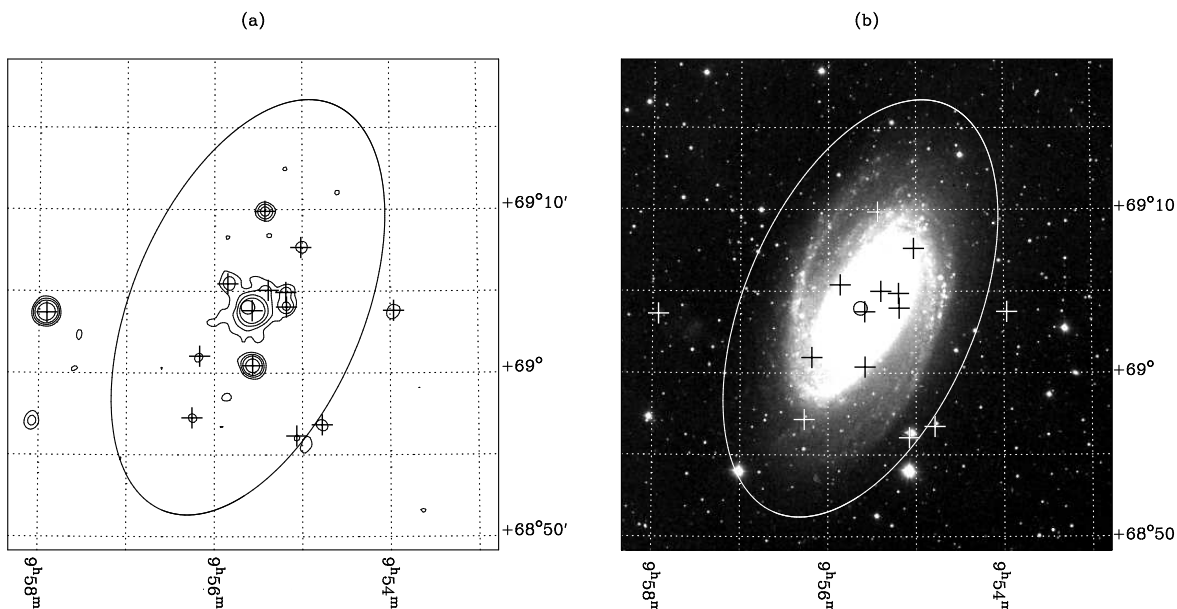
The parent HFS sample is reasonably complete in statistical terms (see Ho, Filippenko & Sargent 1995) and can certainly be considered as representative of the nearby bright galaxy population. However, our XHFS sample is subject to additional selection biases arising both from the selection criteria noted above and from the fact that quite a high fraction of the galaxies (78%) were the actual target source of the HRI observation. Thus nearby galaxies, known to be X-ray bright on the basis of pre-*ROSAT* observations, will be well represented in the XHFS sample, as will established X-ray luminous categories of object such as Seyfert galaxies. Table 1 gives details of how the full HFS sample of galaxies are distributed by morphological type and nuclear properties and, for comparison, provides the same information for the XHFS subset. In terms of galaxy morphology, late-type spirals/irregular galaxies appear to be somewhat favoured. Also, as expected, a relatively high fraction of the Seyfert galaxies in the HFS sample were observed by the HRI (*i.e.* a 29% fraction compared to a norm for all types of galaxy of $\sim 17\%$), although in numerical terms the excess coverage amounts to only about 6 objects. Despite these clear emphases in the XHFS sample, the different morphological types and nuclear classes are, nevertheless, reasonably well sampled by the HRI database. We conclude that the XHFS sample is representative of the range of galaxies that occupy the nearby Universe (except for giant ellipticals and lenticulars) although possibly subject to a bias towards high X-ray luminosity systems.

The individual galaxies contained within the XHFS sample are listed in Table 2, together with brief details relating to the *ROSAT* HRI observations and the galaxy properties.

The point source searching was conducted using the PSS algorithm, which is part of the STARLINK ASTERIX software package (Allen 1995). A circular area of $15'$ radius about the field centre was searched in each case and all discrete X-ray sources with a detection significance of $\geq 5 \sigma$ above a smoothed background level were recorded. The source positions were then plotted on the X-ray image and a visual “quality” check of each detected source was carried out. Sources were flagged as “on-galaxy” or “off-galaxy” dependent upon whether they resided inside or outside of the optical extent of the galaxy. The optical extent was defined in terms of the D_{25} ellipse (*i.e.* the elliptical contour best corresponding to the 25 magnitude/arcsec 2 blue isophote) using the major axis diameter and nuclear position from Ho, Filippenko & Sargent (1997a), and the position angle and axial ratio from the Third Reference Catalogue of Bright Galaxies (RC3; de Vaucouleurs et al. 1991). In this manner a total of 327 discrete X-ray sources were detected coincident with the galaxies in our sample. Figure 1 illustrates this process in the case of NGC 3031 (M81).

Table 1. The distribution with morphological and nuclear type in the full HFS sample compared to that in the XHFS subset.

Hubble type	Galaxy Morphology				Type of Nucleus			
	T	Number of Galaxies			Classification	Number of Galaxies		
		HFS	XHFS	Coverage		HFS	XHFS	Coverage
E	-6 \rightarrow -4	57	9	0.16	Seyferts	52	15	0.29
SO	-3 \rightarrow -1	88	10	0.11	LINERs	159	26	0.16
SO/a - Sab	0 \rightarrow 2	77	15	0.19	(pure	94	15	0.16)
Sb - Sbc	3 \rightarrow 4	103	18	0.17	(transition	65	11	0.17)
Sc - Scd	5 \rightarrow 6	109	16	0.15	H II	206	32	0.16
Sd and later	7 \rightarrow 99	52	15	0.29	NoEL	69	10	0.14
Total		486	83	0.17	Total	486	83	0.17


Figure 1. (a) A contour map of the image derived from the first *ROSAT* HRI observation of NGC 3031 (M81). The point X-ray sources detected by the PSS algorithm are marked with crosses. (b) The position of the point X-ray sources superimposed on the DSS optical image. In both panels the position of the optical nucleus is marked by the circle (25'' radius) and the ellipse represents to the D₂₅ blue isophote.

Since a considerable proportion (24/83) of our galaxies were observed on at least two separate occasions, many of these detections represented repeat observations of the same X-ray sources. We therefore compressed the source list to a “definitive” list of detections by considering all sources positionally coincident to within 15'' in separate observations of the same galaxy, to be the same source (see §3.1)*. This led to a final set of 187 discrete X-ray sources, the catalogue of which is presented in Appendix A.

Visual inspection suggests the presence of diffuse X-ray flux in a small fraction of the HRI images considered above. Most notably there are five cases where a bright point-like X-ray source, positionally coincident with the optical nucleus of the galaxy, appears to be embedded in an extended, low surface brightness component. NGC 3031 in Figure 1(a) pro-

vides one such example, the others being NGC 4151, NGC 4258, NGC 4291 and NGC 4736. We have not specifically flagged extended emission in our analysis and, in fact, ignore its contribution to the X-ray luminosity of the XHFS galaxies, focussing our attention solely on individual discrete (point-like) X-ray sources associated with nearby galaxies. (In all cases any correction for the the extended luminosity detected by the HRI would be much less than a factor 2).

All fluxes (and hence luminosities) quoted in this paper are for the 0.1–2.4 keV *ROSAT* HRI band, corrected for the line-of-sight absorption of our Galaxy. The conversion from measured HRI count rate to unabsorbed flux was calculated for a specific spectral form, namely a power-law continuum with photon index $\Gamma = 2$. The absorption correction is, in most cases, small (less than a factor 2 upwards) since the galaxies in our sample are generally in regions of low Galactic column density ($N_{\text{H}} < 5 \times 10^{20}$ atoms cm^{-2}). The count rate to flux conversion factor is sensitive to the choice of spectral model, for example a change to a thermal bremsstrahlung form with $kT = 1$ keV leads to a 20% reduction in the assigned fluxes.

* We note that in correlating the multiple detections we only needed to apply an attitude correction to one field, namely NGC 4258 A, which required corrections of $\Delta\text{RA} = +1.35^\circ$, $\Delta\text{Dec} = +16.5''$ (calibrated by a bright off-axis source).

Table 2. Details of the 83 galaxies in the XHFS sample. Repeat observations of a galaxy are ordered by epoch and labelled alphabetically. Values of the distance, d , Hubble type, T , and nuclear class are taken from Ho, Filippenko & Sargent (1997a). The foreground (Galactic) column density, N_{H} , in the direction of each galaxy is based on an interpolation of the HI measurements of Stark et al. (1992).

Galaxy	Obs N_{O}	<i>ROSAT</i> data	Exposure (s)	d (Mpc)	N_{H} (10^{20} cm^{-2})	Hubble type, T	Nuclear class	Total XRS	Nuclear XRS?
IC 10	A	rh600902n00	32678	1.3	48.1	10.0	H	1	
	B	rh600902a01	38564						
NGC 147		rh400744n00	14745	0.7	10.5	-5.0		-	
NGC 185		rh400743n00	21070	0.7	11.0	-5.0	S2	1	
NGC 205		rh600816n00	28145	0.7	6.7	-5.0		2	
NGC 221		rh600600n00	12658	0.7	6.5	-6.0		2	y
NGC 404		rh703894n00	23874	2.4	5.1	-3.0	L2	1	y
NGC 520	A	rh600628n00	13454	27.8	3.3	99.0	H	-	
	B	rh600628a01	18538						
NGC 891		rh600690n00	98118	9.6	6.8	3.0	H	5	
NGC 1058		rh500450n00	60796	9.1	5.6	5.0	S2	-	
IC 342		rh600022n00	19147	3.0	30.3	6.0	H	7	y
NGC 1560		rh702727n00	17501	3.0	11.4	7.0	H	-	
NGC 1569		rh600157n00	11350	1.6	24.2	10.0	H	1	y
NGC 1961		rh600499n00	82704	53.1	8.5	5.0	L2	1	y
NGC 2276	A	rh600498n00	52235	36.8	6.0	5.0	H	1	
	B	rh600498a01	21731						
NGC 2366		rh702732n00	31823	2.9	3.9	10.0		-	
NGC 2403		rh600767n00	26544	4.2	4.1	6.0	H	4	
NGC 2775	A	rh500385n00	10892	17.0	4.3	2.0		-	
	B	rh600826a01	48468						
NGC 2782		rh700462n00	21715	37.3	1.8	1.0	H	2	y
NGC 2903		rh600602n00	13619	6.3	3.4	4.0	H	3	y
NGC 2976	A	rh600471n00	18801	2.1	4.5	5.0	H	1	
	B	rh600759n00	26524						
	C	rh600759a01	23443						
NGC 3031	A	rh600247n00	26558	1.4	4.3	2.0	S1.5	20	y
	B	rh600247a01	21263						
	C	rh600739n00	20080						
	D	rh600740n00	19163						
	E	rh600881n00	14934						
	F	rh600882n00	18508						
	G	rh601001n00	19420						
NGC 3079	A	rh700100n00	21005	20.4	0.9	7.0	S2	1	y
	B	rh600411n00	20676						
	C	rh700889n00	18677						
	D	rh701294n00	25330						
	E	rh702425n00	25077						
NGC 3073		rh600411n00	20676	19.3	0.9	-2.5	H	-	
NGC 3147	A	rh600614n00	23438	40.9	3.2	4.0	S2	1	y
	B	rh600721n00	22582						
	C	rh600721a01	26308						
NGC 3185		rh800844n00	29237	21.3	2.2	1.0	S2:	-	
NGC 3190		rh800844n00	29237	22.4	2.1	1.0	L2	1	y
NGC 3193		rh800844n00	29237	23.2	2.1	-5.0	L2:	-	
NGC 3226		rh701299n00	30264	23.4	2.3	-5.0	L1.9	1	y
NGC 3227		rh701299n00	30264	20.6	2.3	1.0	S1.5	1	y
NGC 3294		rh500389n00	11288	26.7	1.6	5.0	H	-	
NGC 3310		rh600685a01	41842	18.7	1.1	4.0	H	2	
NGC 3377		rh600830n00	34272	8.1	2.9	-5.0		2	y
NGC 3379		rh600829n00	24560	8.1	2.9	-5.0	L2/T2::	1	y
NGC 3384		rh600829n00	24560	8.1	2.9	-3.0		-	
NGC 3389		rh600829n00	24560	22.5	2.8	5.0	H	-	
NGC 3395		rh600771n00	24925	27.4	1.8	6.0	H	1	
NGC 3628		rh700009n00	13574	7.7	2.0	3.0	T2	2	
NGC 3998		rh600430n00	13622	21.6	1.2	-2.0	L1.9	2	y
NGC 4051		rh701298n00	10579	17.0	1.3	4.0	S1.2	1	y
NGC 4088		rh500391n00	10017	17.0	2.0	4.0	H	1	y
NGC 4150		rh600762a01	10457	9.7	1.6	-2.0	T2	1	y

Galaxy	Obs N _g	ROSAT data	Exposure (s)	<i>d</i> (Mpc)	<i>N</i> _H (10 ²⁰ cm ⁻²)	Hubble type	Nuclear class	Total XRS	Nuclear XRS?
NGC 4151	A	rh701707n00	108216	20.3	2.1	2.0	S1.5	3	y
	B	rh701989n00	103435						
NGC 4203		rh600221n00	25447	9.7	1.3	-3.0	L1.9	1	y
NGC 4214		rh600741n00	42584	3.5	1.7	10.0	H	1	
NGC 4235		rh600412a01	19694	35.1	1.5	1.0	S1.2	1	y
NGC 4258	A	rh701008n00	27556	6.8	1.4	4.0	S1.9	8	y
	B	rh600599a01	25562						
NGC 4291	A	rh600441n00	12405	29.4	3.2	-5.0		1	y
	B	rh600834n00	35363						
NGC 4321		rh600731n00	42797	16.8	2.4	4.0	T2	4	y
NGC 4388		rh700192n00	11274	16.8	2.7	3.0	S1.9	1	y
NGC 4395		rh702725n00	11353	3.6	1.3	9.0	S1.8	1	
NGC 4435		rh600608n00	21651	16.8	2.7	-2.0	T2/H	1	y
NGC 4438		rh600608n00	21651	16.8	2.7	0.0	L1.9	1	y
NGC 4449	A	rh600743n00	15373	3.0	1.3	10.0	H	7	y
	B	rh600865n00	25395						
	C	rh600865a01	18343						
NGC 4470		rh600216a01	27367	31.4	1.6	1.0	H	-	
NGC 4485	A	rh600855n00	27048	9.3	1.8	10.0	H	1	y
	B	rh600855a01	24829						
NGC 4490	A	rh600855n00	27048	7.8	1.8	7.0	H	4	y
	B	rh600855a01	24829						
NGC 4527		rh500390n00	10355	13.5	1.9	4.0	T2	-	
NGC 4559		rh600861n00	53812	9.7	1.5	6.0	H	5	y
NGC 4569		rh600603a01	21858	16.8	2.5	2.0	T2	1	y
NGC 4631	A	rh600193a01	14287	6.9	1.3	7.0	H	2	
	B	rh600193a02	12041						
NGC 4638	A	rh600480a01	11915	16.8	2.4	-3.0		-	
	B	rh600620a01	19923						
NGC 4647	A	rh600480a01	11915	16.8	2.4	5.0	H	-	
	B	rh600620a01	19923						
NGC 4651		rh800719n00	25396	16.8	2.0	5.0	L2	1	y
NGC 4656		rh600605n00	27668	7.2	1.3	9.0	H	1	
NGC 4736	A	rh600678n00	112910	4.3	1.4	2.0	L2	5	y
	B	rh600769n00	27292						
NGC 4772		rh500397n00	12120	16.3	1.8	1.0	L1.9	-	
NGC 4826		rh600715n00	10150	4.1	2.6	2.0	T2	1	y
NGC 5005		rh701711n00	26742	21.3	1.1	4.0	L1.9	1	y
NGC 5055		rh600742n00	12343	7.2	1.4	4.0	T2	9	y
NGC 5194		rh600601n00	36323	7.7	1.5	4.0	S2	9	y
NGC 5195		rh600601n00	36323	9.3	1.5	90.0	L2:	1	
NGC 5204	A	rh702723n00	14852	4.8	1.5	9.0	H	1	y
	B	rh702723a01	13675						
NGC 5273		rh701006n00	10767	21.3	0.9	-2.0	S1.5	1	y
NGC 5354		rh800743n00	22761	32.8	1.0	-2.0	T2/L2:	-	
NGC 5457	A	rh600092n00	18588	5.4	1.2	6.0	H	27	
	B	rh600383n00	32624						
	C	rh600820n00	108850						
	D	rh600820a01	68872						
NGC 5775		rh600964n00	35305	26.7	3.3	5.0	H	-	
NGC 5850	A	rh600478n00	22796	28.5	4.2	3.0	L2	-	
	B	rh600478a01	16763						
NGC 5905		rh703855n00	76218	44.4	1.4	3.0	H	1	y
NGC 6217	A	rh141910n00	15991	23.9	4.1	4.0	H	1	y
	B	rh141913n00	14669						
	C	rh141921n00	13572						
	D	rh141926n00	11804						
	E	rh141928n00	11630						
NGC 6503		rh600618n00	14787	6.1	4.0	6.0	T2/S2:	1	
NGC 6654	A	rh600124a00	36803	29.5	5.4	0.0		-	
	B	rh600124a01	18270						
NGC 6946	A	rh600501n00	60305	5.5	20.2	6.0	H	13	y
	B	rh600718n00	21723						
NGC 7331		rh702074n00	30481	14.3	7.7	3.0	T2	1	y

3 PRELIMINARY ANALYSIS OF THE XHFS SAMPLE

3.1 Nuclear versus non-nuclear source designation

As a first step in the analysis we have attempted to separate out those X-ray sources possibly associated with the nuclei of the XHFS galaxies from the other constituent X-ray source populations. The reason for this is that an active galactic nucleus (AGN) is known or suspected to be present in quite a number of the galaxies in our sample and, more often than not, is the dominant source of X-ray emission in the nuclear region and sometimes in the whole galaxy (examples include NGC 4736, Roberts, Warwick & Ohashi 1999; NGC 3031, Ishisaki et al. 1996; NGC 3147, Ptak et al. 1997). Since, as far as we know, galaxies contain at most one AGN located close to the mass centroid of the galaxy, then there is clearly some logic in differentiating between “nuclear” and “non-nuclear” sources.

In the present study the identification of a particular X-ray source with the nucleus of a galaxy is based solely on a positional coincidence criterion. In *ROSAT* HRI observations there is the potential for systematic pointing errors of up to $\sim 10''$ (see Harris et al. 1998) in addition to statistical errors of up to $\sim 5''$ (dependent on the source strength). For example, in the case of NGC 3079, we observe the position of one particular source (designated NGC 3079 X-1 in Appendix A) to shift by up to $15''$ in 5 separate observations. There is also some uncertainty in the position of the optical nucleus; Ho, Filippenko & Sargent (1995) only quote their nuclear positions to one second of time implying a potential error of up to $7.5''$. This would suggest that a reasonable criterion for designating an X-ray source as “nuclear” would be if it lies within $\sim 20''$ of the optical nucleus. In fact the observations reveal a total of 40 X-ray sources with an offset from the optical nucleus of less than $20''$, with a further 5 sources lying in the $20 - 25''$ range. However, 4 out of these 5 sources have an X-ray luminosity in excess of the median value for all the galactic nuclei and, considering this along with the detection of some probable AGN out to $\sim 20''$ from the optical nuclear position, we therefore set a very *conservative* limit of $25''$ as a threshold radius (thereby avoiding any possible contamination of the non-nuclear sample by AGN). Hereafter we refer to any sources seen within this bound as “nuclear” X-ray sources and label those outside this region as “non-nuclear” X-ray sources.

The division of the XHFS sample into nuclear and non-nuclear X-ray sources is illustrated in Figure 2. One point that is apparent immediately from this figure is that relatively high luminosity ($L_X \gtrsim 10^{39}$ erg s $^{-1}$) sources are not confined solely to the nuclear region, in fact such sources are seen at projected distances from the optical nucleus ranging from less than a few hundred pc (*i.e.* positional coincident with the nucleus in terms of the measurement errors) out to beyond 10 kpc. In a recent paper exploiting *ROSAT* HRI observations, Colbert & Mushotzky (1999), have suggested the possibility that some nearby spiral galaxies contain X-ray sources powered by accretion onto black holes with masses of typically $10^2 - 10^4 M_\odot$. These authors invoke the existence of a black-hole population in this intermediate mass range (compared to the Galactic black-hole binaries with masses typically $\sim 10 M_\odot$ and luminous AGN with $M \sim 10^6 - 10^9 M_\odot$) to explain why X-ray sources with

luminosities of $L_X \sim 10^{40}$ erg s $^{-1}$ are occasionally observed in spiral galaxies with a significant positional offset from the optical nucleus. In fact Colbert & Mushotzky quote a mean offset of ~ 390 pc between the X-ray source position and the optical photometric center for the 21 galaxies with X-ray detections in their sample[†]. In Figure 2 there is no real evidence for the more luminous sources to be grouped preferentially within a projected separation of 1 kpc but such an effect, if present, might well be smeared out by the positional errors. Colbert & Mushotzky (1999) concentrate on a set of galaxies with recessional velocity less than 1000 km s $^{-1}$ (*i.e.* a *very nearby* sample) and hence benefit from the better effective linear resolution.

We find that 45 galaxies out of 83 in the XHFS sample harbour a nuclear X-ray source. The corresponding statistic for the non-nuclear X-ray sources is that 34 of the XHFS galaxies contain at least one such source. There were no X-ray detections in 21 of the XHFS galaxies.

In Figure 3 (panels a & b) we present histograms of the observed luminosity distribution for the 187 sources in the XHFS sample separated into the non-nuclear and nuclear categories. Figure 3(b) also includes 95% upper limits on the X-ray luminosity of the nuclear emission for the 38 galaxies with no detected nuclear X-ray source (these upper limits are tabulated in Appendix B). Although the luminosity distributions for the two populations overlap, on average the *detected* nuclear X-ray sources are substantially more X-ray luminous than the non-nuclear sources (the median X-ray luminosity of the former being 5.4×10^{39} erg s $^{-1}$ as opposed to 2.8×10^{38} erg s $^{-1}$ for the latter).

It should be emphasized that the X-ray sources designated as nuclear are not necessarily all low-luminosity AGN. Indeed, since the range of X-ray luminosity exhibited by the non-nuclear sources shows a significant overlap with the nuclear sample, some contamination of the latter category by non-AGN looks inevitable. The problem of distinguishing very low-luminosity AGN from individual black hole X-ray binaries, groupings of Eddington-limited low-mass XRBs and recent X-ray luminous supernovae is, of course, well recognised (*e.g.* Dahlem, Heckman & Fabbiano 1995; Loewenstein et al. 1998; Lira et al. 1999). However the above argument does not preclude the possibility that many of the nuclear X-ray sources contained in the XHFS sample are putative low-luminosity AGN, particularly if the underlying population of super-massive black holes have a very wide range of masses and/or accretion rates (Colbert & Mushotzky 1999).

3.2 Contamination of the XHFS sample by background QSOs and/or foreground stars

A potential source of uncertainty is the detection of either foreground sources or background sources which lie, by chance, within the D_{25} ellipse of one of the XHFS galaxies. Such contamination is likely to be much more of a problem for the non-nuclear category since, in this case, the total sky area surveyed amounts to almost exactly one square degree (with the area within the nuclear error circles accounting for

[†] A total of 11 out of the 39 galaxies studied by Colbert & Mushotzky (1999) overlap with our XHFS sample

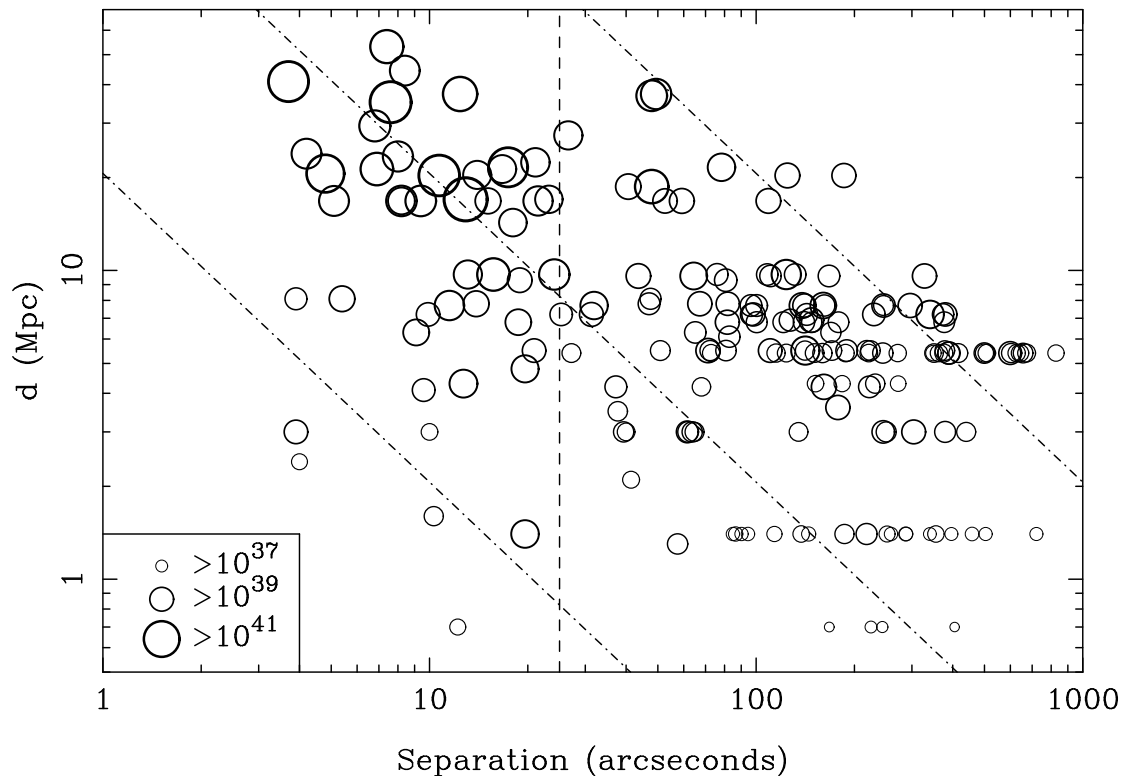


Figure 2. The observed separation of the 187 X-ray sources from the position of the optical nucleus of the host galaxy. The vertical (dashed) line drawn at a separation of $25''$ divides the sources classified as “nuclear” from those considered to be “non-nuclear”. The three diagonal (dot-dash) lines correspond to projected linear scales of 100 pc, 1 kpc and 10 kpc. The luminosity of each source is represented by the size of its circle as illustrated in the inset.

only $\sim 1\%$ of this figure). At the flux limits reached in the present survey (see below), most of the contamination is due to late-type stars in our own Galaxy and distant QSOs (the latter representing the dominant X-ray source population in medium-deep *ROSAT* images).

In Figure 4(a) we show the distribution of non-nuclear source detections as a function of the observed X-ray flux. We have carried out a quantitative investigation of the contamination of the non-nuclear population expected at different flux levels using two independent approaches. Firstly we estimated the level of contamination in each HRI field using the detections outside of the D_{25} ellipse of the target galaxy but within the nominal HRI field of view as a control set. After applying an appropriate field by field scaling of the number of off-galaxy detections[‡], we obtain an estimate of the number of false associations expected as a function of flux as illustrated in Figure 4(b). Comparison of the observed distribution with this estimate demonstrates that the contamination of the non-nuclear XHFS sample is

[‡] The weighting factor was simply the ratio of the on-galaxy to off-galaxy area for the field; here and elsewhere in this paper we neglect vignetting and other effects which reduce the point-source sensitivity at the edge of the HRI field of view compared to that at the centre by about 10%.

at a level of no more than about 13%. As an additional check we also performed a calculation based on published source counts for the soft X-ray band. First the X-ray source detection limit for each field was estimated and the integrated sky area encompassed in the XHFS (within the D_{25} ellipses of the XHFS galaxies) determined as a function of the limiting X-ray flux - see Figure 4(c). The differential form of the $\log N - \log S$ relation derived by Hasinger et al. (1993), which includes contributions from both QSOs and Galactic stars, was then folded through this coverage curve to give the predicted number of sources shown in Figure 4(d). The contamination level determined from the second method is 11%, very comparable, within the statistics, to that obtained from the first.

There are two caveats relating to this comparison of observed and predicted source numbers. The effect of absorption by cool gas and dust contained within the galaxy disks will help suppress the detection rate of background QSOs, implying that both of the estimates above actually give upper limit predictions. A second possibility is that the measured off-galaxy detection rate may be biased upwards by sources actually associated with the target galaxy but lying outside its D_{25} contour. This latter influence could give rise to the slight differences between the two predicted distributions in Figure 4, but clearly the evidence for any such effects is very marginal. In summary we can be confident that

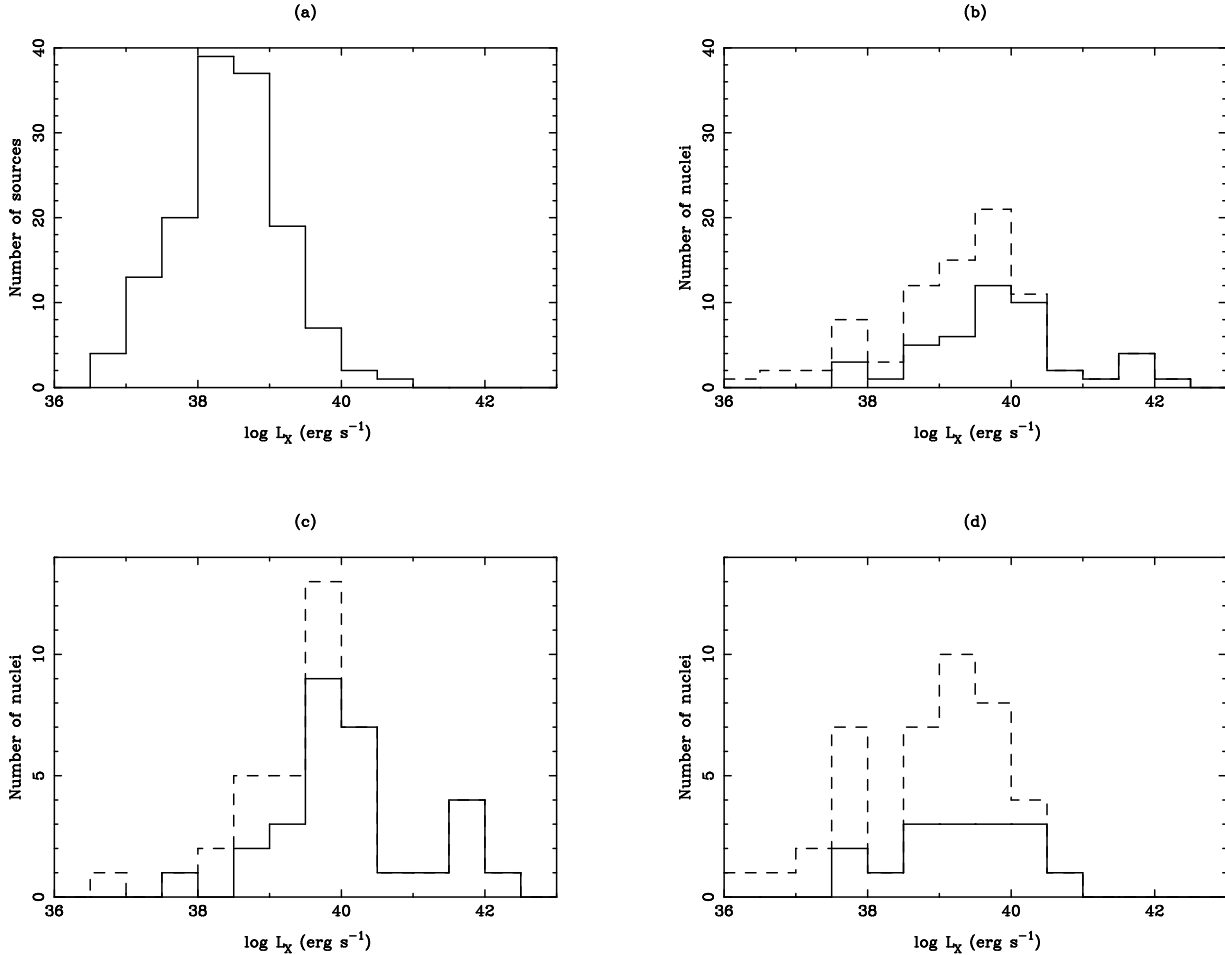


Figure 3. The distribution of X-ray luminosity exhibited by sources in the XHFS sample. (a) The non-nuclear sources. (b) The nuclear sources. The dashed histogram shows the effect of including the 95% upper limits for the galaxies with no detected nuclear X-ray source. (c) Same as (b) but restricted to galaxies with Seyfert or LINER nuclei. (d) Same as (b) but restricted to galaxies with H II nuclei or no nuclear emission lines.

the great majority (in excess of 85%) of the non-nuclear X-ray sources in our sample are associated with HFS galaxies. We also confirm that there is essentially no contamination of the nuclear source sample, since we expect a total of ~ 0.2 sources coincident by chance compared to the 45 sources we detect.

As a final point we note that if we transpose the distributions in Figure 4(b,d) into luminosity space using the appropriate galaxy distances (on a field by field basis), then the distribution in luminosity (of the contamination) is very comparable to that exhibited by the non-nuclear sources in Figure 3(a). We conclude that the high luminosity tail of non-nuclear sources is not due to contamination by foreground or background sources but represents a real super-luminous population associated with nearby galaxies.

4 PROPERTIES OF THE NUCLEAR SAMPLE

The search for “dwarf” Seyfert nuclei carried out by Ho, Filippenko & Sargent (1995, 1997a,b,c) has resulted in a con-

sistent and complete classification of the optical emission line properties of each galactic nucleus in the HFS galaxy sample. They found that 11% of nearby galaxies harbour a Seyfert-like nucleus, 33% host a Low Ionisation Nuclear Emission-line Region (LINER) and 42% have a nucleus with an emission line spectrum characteristic of H II regions. The LINERs may be further split into the subsets of “pure” LINERs (19% of the HFS sample) and “transition” LINERs (14%), the difference being that the transition objects display a blend of LINER and H II spectra. Only 14% of galaxies appear to have nuclear spectra devoid of optical emission lines (which are referred to here as “NoEL” nuclei).

As noted earlier (see Table 1) the XHFS sample encompasses the full range of nuclear spectral classification, thus allowing us to consider the X-ray properties, specifically the soft X-ray luminosities, of the different types of nucleus. Figure 3 (panels c & d) compares the X-ray luminosity distribution for those galaxies with Seyfert or LINER nuclei to those with H II spectra or no emission lines. Table 3 gives further details of the mean nuclear X-ray luminosity

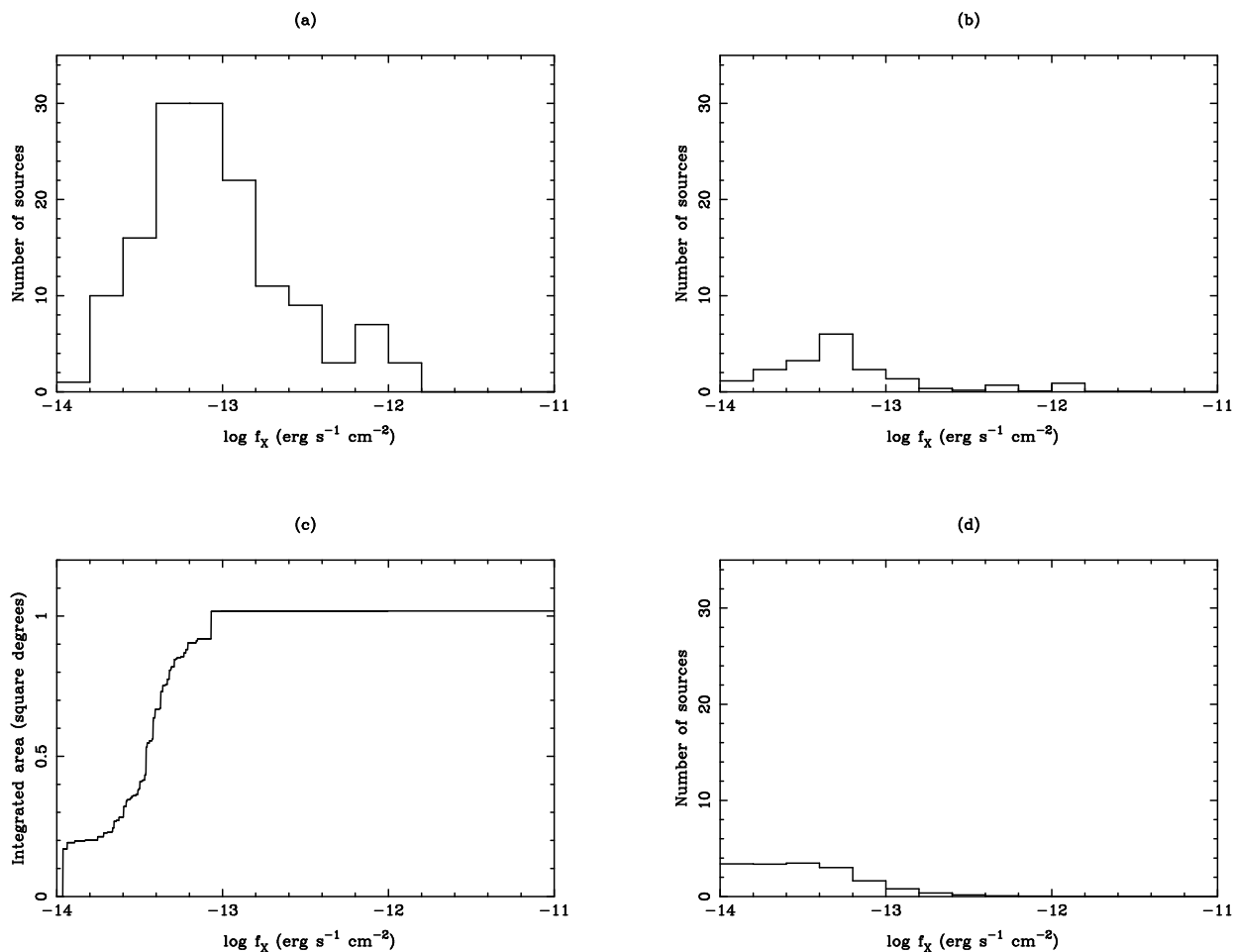


Figure 4. (a) The observed flux distribution of the non-nuclear X-ray sources. (b) The predicted flux distribution for contaminating sources based on the off-galaxy detections. (c) The sky coverage (within the galaxy D₂₅ contours) versus the limiting flux. (d) The predicted flux distribution of contaminating sources derived from the differential X-ray source counts of Hasinger et al. (1993).

Table 3. The mean X-ray luminosities and detection rates of various optically-defined categories of nuclei.

Sample	No. of Objects	Mean $\log L_X$ (erg s ⁻¹)	Detection rate (%)
All nuclei	83	38.93 ± 0.15	54
Seyferts & LINERs	41	39.51 ± 0.22	71
HII & NoEL	42	38.36 ± 0.17	42
Seyferts	15	39.83 ± 0.43	73
LINERs	26	39.36 ± 0.22	69
(pure	15	39.49 ± 0.32	73)
(transition	11	39.28 ± 0.18	64)
H II	32	38.48 ± 0.20	41
NoEL	10	38.02 ± 0.30	30
Broad Line AGN	15	40.38 ± 0.30	87
Narrow Line AGN	26	39.05 ± 0.24	62

and detection rate for various sub-groupings in the XHFS sample.[§]

For the overall sample the average X-ray luminosity is $\sim 10^{39}$ erg s⁻¹. However, a marked difference is seen between those nuclei probably hosting a low-luminosity AGN (the Seyfert and LINER nuclei) and those showing no evidence for high-ionization emission lines (the H II and NoEL galaxies). Essentially, we observe the former to be considerably more luminous than the latter. This manifests itself as both a higher X-ray luminosity (by a factor ~ 10) and a higher detection rate of nuclear sources. A formal comparison of the two distributions shown in Figure 3 (panels c & d) using the two-sample tests in the **ASURV** package confirms that the distributions are different at a significance level greater than 99.9%.

Within the putative AGN grouping, there is little to distinguish Seyfert from LINER nuclei in terms of either their average luminosity, detection rate or the luminosity spread. When the LINERs are divided into “pure” and “transition” types, the former are seen to bear a slightly closer resemblance to the Seyferts, in terms of their X-ray characteristics, than the latter (although the differences are at a marginal significance level). The galaxies with broad emission lines (the “type 1” AGN), discussed by Ho, Filippenko & Sargent (1997b), are clearly the most luminous group of objects in the XHFS sample having an X-ray luminosity at least an order of magnitude larger than the narrow-emission line (“type 2”) sources and a higher detection rate. Nevertheless the average luminosity of the type 2 objects is still well in excess of that of the H II and NoEL galaxies (formally the log L_X distributions are different at a significance level of 98%). We conclude that X-ray emission associated with an underlying low-luminosity AGN is seen in almost all of the nearby galactic nuclei classified as type 1 Seyferts or LINERs and in a reasonable fraction ($\sim 60\%$) of those nuclei classified as type 2 objects. Since obscuration in the line of sight to the nucleus in type 2 objects will strongly suppress the 0.1–2.4 keV flux if the column density is in excess of $\sim 10^{22}$ cm⁻², it may be that in many of the type 2 nuclei we actually observe scattered X-ray flux (or some other nuclear related extended component) rather than the direct continuum emission of the nucleus.

The observed distribution of nuclear luminosity in the galaxies categorised as H II or NoEL objects overlaps substantially with that measured for non-nuclear sources in the XHFS sample (Figure 3(a) & (d)). Thus it is quite plausible that in many of the H II and NoEL galaxies with nuclear detections we are, in fact, observing a component of the discrete X-ray source population of the galaxy rather than the presence of an underlying, optically faint, AGN.

The properties of the putative AGN in the XHFS sample may be further investigated by comparing the observed

X-ray luminosity with other indicators of nuclear activity. We examine the relationship between the X-ray and H α luminosity (both narrow and broad components) for the Seyferts and LINERs in Figure 5. The H α luminosities (including lower limits on the narrow component, $L_{H\alpha,n}$, from measurements made in non-photometric conditions) were taken from Ho, Filippenko & Sargent (1997a,b); where no measurement of the broad component, $L_{H\alpha,b}$, is available we use the lower limit on $L_{H\alpha,n}$ and the fractional contribution of broad H α to the total H α emission to derive a lower limit on $L_{H\alpha,b}$.

A correlation between the total H α luminosity and soft X-ray luminosity of high luminosity QSOs and Seyfert I galaxies is well established, and has recently been shown to extend down to $L_X \sim 10^{40}$ erg s⁻¹ by Koratkar et al. (1995). They find that type 1 AGN have a typical $L_X/L_{H\alpha}$ ratio in the range 1 - 100, with a mean of ~ 30 . These results broadly agree with Figure 5, where an apparently similar range of ratios is seen to extend down to $\sim 10^{38}$ erg s⁻¹. Koratkar et al. (1995) show their correlation is present in flux as well in luminosity space. When Figure 5 is replotted in this regime, there is little evidence of a correlation, but this is probably due to the restricted flux range, the degree of scatter being similar to that seen by Koratkar et al. The factors which may induce scatter in the X-ray luminosity at a given H α output include soft X-ray absorption, nuclear flux variability and contamination by the non-AGN X-ray source population of the galaxies (which is clearly a particular problem in the low-luminosity range). The present work demonstrates that the $L_X/L_{H\alpha}$ relationship may extend from $L_X > 10^{46}$ erg s⁻¹ down to $L_X \sim 10^{38}$ erg s⁻¹, two magnitudes lower than previously seen and implies a significant commonality in the physical processes that drive low- and high-luminosity AGN.

Dynamical studies of the centres of nearby galaxies have revealed the presence of Massive Dark Objects (MDOs) in the nuclei of number of galaxies (Kormendy & Richstone 1995). The demographics of this population show that a reasonably tight relationship exists between the masses of the MDOs and the mass of the galactic bulge hosting them (± 0.5 decades standard deviation in the ratio; Magorrian et al. 1998). Since the mass-to-light relationship of these bulges is also known then a mass of the MDO may be inferred from the optical blue bulge luminosity, L_{bulge} , of a galaxy. In the following analysis we make the assumption that these MDOs are most likely supermassive black holes resident in the nucleus of the galaxies; this assumption, and caveats relating to the observations of MDOs, are discussed by Lawrence (1999, and references therein).

Applying the Magorrian et al. (1998) relation to the XHFS sample, we can obtain an estimate of the underlying black hole mass, M_{BH} , and hence the fraction of Eddington luminosity at which any particular XHFS nucleus is radiating. Ho, Filippenko & Sargent (1997a) provide an estimate of the bulge magnitude of each galaxy in their sample, formulated from an average, type-dependent relation of the form discussed by Whittle (1992). By definition all light from ellipticals is assumed to come from the bulge (since they have no disk); the correction to bulge luminosity from that of the full galaxy then ranges, for example, from 1.02 mag for Sa galaxies to 2.54 mag for Sc galaxies. Figure 6 shows a plot of the nuclear L_X versus L_{bulge} for the Seyferts and LINERs in

[§] We have calculated the mean value of log L_X and the associated error using the Kaplan-Meier estimator procedure in the **ASURV** software package (Rev 1.2), which takes account of both the actual measurements and upper-limits (see Feigelson & Nelson 1985). Prior to applying the estimator a few upper-limits below log $L_X = 37.5$ were reset to this minimum value. In some cases the lowest value in the distribution was an upper-limit resulting in a (probably modest) upward biasing of the mean.

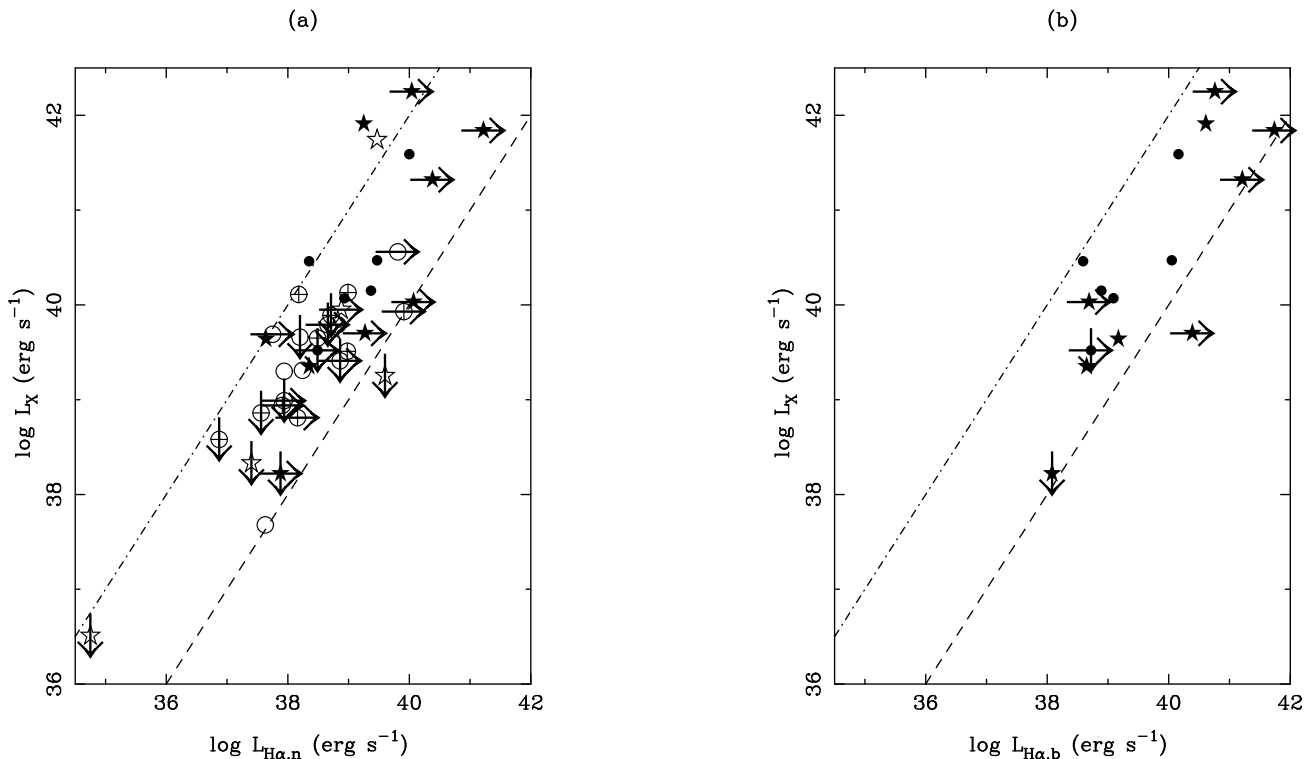


Figure 5. Scatter plots of the nuclear X-ray luminosity, L_X versus the nuclear $H\alpha$ luminosity (a) for the narrow component of $H\alpha$, (b) for the broad component of $H\alpha$. In both panels Seyferts are marked by stars and LINERs by circles, with the broad-line examples of either type of object shown by a filled-in symbol. The transition LINERs are indicated by a crossed circle. Limits are indicated by arrows through the symbols. Ratios of $L_X/L_{H\alpha}$ of 1 and 100 are shown by the dashed and dot-dash lines respectively.

the XHFS sample. The diagonal lines calibrate the measurements in terms of the fraction of the Eddington luminosity, based on the M_{BH} to L_{bulge} relation from Magorrian et al. Here we assume that the X-ray emission in the *ROSAT* 0.1–2.4 keV band amounts to 15% of the bolometric luminosity of the AGN, which we estimate from the spectral energy distributions of low-luminosity AGN (specifically those in spirals) presented by Ho (1999). The AGN in the XHFS sample would all appear to be radiating at severely sub-Eddington luminosities, the highest rate being $\sim 10^{-3}$ of the Eddington value, but with $\sim 10^{-6}$ a more typical figure.

There are, of course, several factors that could induce a bias in these measurements. Firstly, considerable absorption in the *ROSAT* band could easily suppress the observed luminosity by a factor $\sim 10^2$; for example, in classical type 2 sources in which the direct line of sight to the nucleus is completely blocked, a scattered nuclear flux amounting to $\sim 1\%$ of the direct nuclear continuum is often observed (*e.g.* Turner et al. 1997). However, many of the sources with extremely low rates are type 1 nuclei, which in general do not exhibit substantial soft X-ray absorption due to cold gas intrinsic to the source (*e.g.* George et al. 1998). Another potential problem is that the mass estimates (in the range $10^6 - 10^9 M_\odot$) for the underlying supermassive black holes

powering these relatively low-luminosity Seyfert and LINERs may be unrealistic. The Magorrian et al. (1998) sample is comprised predominantly of giant elliptical and lenticular galaxies (a population which is specifically excluded from the current work, see §2). Wandel (1999) has pointed out the potential bias in the dynamical measurement towards galaxies harbouring particularly massive black holes. In fact, Wandel (1999) presents results showing that black hole masses in Seyfert nuclei (inferred via a reverberation mapping/virial mass technique) are generally smaller by a factor ~ 20 than those obtained using the Magorrian et al. relation. Plausibly this downward scaling could be even greater for galaxies with low-luminosity nuclei. This is supported by Salucci et al. (1999), who use kinematic observations of the innermost regions of spiral galaxies to demonstrate that late-type spirals (types Sb - Im) may contain under-massive MDOs, for a given bulge mass, when compared to ellipticals and early-type spirals.

However, even if we apply a rather arbitrary upward scaling to our derived Eddington fractions of, say, 10^2 to account for the above uncertainties, we are still left with the bulk of the XHFS AGN sample operating in a substantially sub-Eddington regime, implying accretion rates firmly in the range theorised for advection-dominated accretion flows

(ADAFs; Narayan & Yi 1995; Fabian & Rees 1995). Colbert & Mushotzky (1999) discuss the ADAF scenario and an alternative approach, namely that low-luminosity AGN found in nearby galaxies might be powered by a new class of intermediate mass black holes ($10^2 - 10^4 M_\odot$), accreting in their soft state. It should be noted, though, that this latter hypothesis does not hold in the case of nearby galaxies where an MDO mass is known, for example NGC 4594 (Fabiano & Juda 1997). Yet a further variation, suggested by Siemiginowska et al. (1996), is that ionisation instability in the accretion disks around super-massive black holes leads to long periods of quiescence, during which accretion occurs at a severely sub-Eddington rate; in this scenario LLAGNs might correspond to systems exhibiting an extended “low state”.

5 PROPERTIES OF THE NON-NUCLEAR SAMPLE

Non-nuclear X-ray sources have been detected in 34 out of the 83 galaxies in the XHFS sample. These sources range in luminosity from $\sim 10^{36.5}$ to $\sim 10^{41}$ erg s $^{-1}$ in the 0.1–2.4 keV band as illustrated in Figure 3(a). Here we investigate the true form of the high luminosity end of the X-ray luminosity distribution for discrete sources in galaxies (excluding low-luminosity AGN). Specifically we focus on discrete X-ray sources detected in spiral galaxies of type SOa to Scd ($T = 0 - 6$), which provide the bulk of the non-nuclear sources in our sample (120 out of 142 sources).

Since the effective sensitivity in terms of L_X varies from galaxy to galaxy, it is necessary to apply a correction for the varying survey coverage. For each *ROSAT* HRI field we transposed the threshold flux for point source detection (as calculated in §3.2) to luminosity using the distance of the XHFS target galaxy and then constructed a cumulative coverage curve as a function of increasing (threshold) X-ray luminosity. To allow for the considerable spread in absolute magnitude across the 49 galaxies which comprise the XHFS spiral sample (this includes the spirals with no non-nuclear source detections), each galaxy was given a weight proportional to its optical B-band luminosity; specifically we use a weight factor equal to L_B in units of $10^{10} L_\odot$. The resulting coverage curve is shown in Figure 7(a). The “true” distribution in luminosity was calculated by binning the observed source sample in terms of L_X (in half-decade logarithmic steps) and then correcting the number of sources in each bin, N_i , for the effective coverage. The result was the differential luminosity distribution shown in Figure 7(b) which, in effect, represents an average per $10^{10} L_\odot$ of optical blue luminosity. The error bars are simply $\pm\sqrt{N_i}$ estimates scaled by the coverage correction.

The XHFS measurements best constrain the discrete X-ray source population of spiral galaxies in the X-ray luminosity range $10^{38.5} - 10^{40.5}$ erg s $^{-1}$. However, information is available for X-ray sources at least two orders of magnitude less luminous, from the extensive surveys of the local group galaxies carried out by *ROSAT*. Here we have used the results on M31 from the *ROSAT* PSPC survey reported by Supper et al. (1997) to extend the measurements in Figure 7(b) down to 10^{36} erg s $^{-1}$. For this purpose we have used the log N - log S curves for X-ray sources detected

in disk areas II, III and IV of M31 (see Figure 14, Supper et al. 1997). We also use the conversion 1 PSPC count s $^{-1} = 1.5 \times 10^{39}$ erg s $^{-1}$ (0.1–2.4 keV) and scale the M31 source numbers to an optical luminosity $L_B = 3.6 \times 10^{10} L_\odot$. Note that the M31 measurements in the lowest bin are shown as a lower-limit since the correction for varying sensitivity across the field of view in the PSPC observations is a significant (and somewhat uncertain) correction at this level of X-ray luminosity.

The measurements in Figure 7(b) indicate a steep, near power-law form for the X-ray luminosity distribution of discrete sources in spiral galaxies. Taking just the XHFS data points and using a simple minimum χ^2 fitting technique, we find that the best fitting straight line in log N(L_X) - log L_X space has a power-law slope of $-1.08^{+0.40}_{-0.22}$. However, when the XHFS data are combined with the M31 measurements a somewhat flatter slope of $-0.78^{+0.07}_{-0.09}$ is obtained. These two best-fitting power-law forms are illustrated in Figure 7(b). The flatter relation appears to be broadly consistent, within the errors, with all the available data although, in this case, there is the hint of a turn down above $L_X \approx 10^{40}$ erg s $^{-1}$. Unfortunately the data quality are such that we cannot rule out the possibility that a break in the power-law occurs at even lower luminosity (*e.g.* at $\sim 10^{39}$ erg s $^{-1}$).

The above analysis is based on the X-ray sources detected within the confines of the optical disc of the sample of spiral galaxies but excludes the sources located within the nominal 25'' nuclear error circle, some of which may well correspond to components of the galactic source population other than low-luminosity AGN. Thus our luminosity distribution strictly represents a lower-limit estimate; fortunately the comparison with M31 is on a similar basis in that the M31 measurements exclude the bulge region, *i.e.* a region within radius 5' (= 1 kpc) of the nucleus of M31. If we include both the nuclear X-ray sources associated with H II and NoEL galaxies (9 sources) and also those associated with Seyfert and LINER nuclei (a further 20 sources), the effect, as expected, is a flattening of the power-law fit to the XHFS data to a slope of $-0.65^{+0.20}_{-0.18}$, a value which changes only marginally when the M31 data are also included. A further potential bias arises, of course, due to the limited angular resolution of the HRI. In this case the effect of closely-spaced discrete sources blending into a single detection, is to induce a flattening of the measured luminosity function. It is quite possible that this latter effect partly compensates for the fact that the nuclear sources are excluded in our primary analysis.

The best-fit straight line to the combined XHFS and M31 datasets in Figure 7(b) corresponds to a differential luminosity distribution of the form $dN/dL_{38} = (1.0 \pm 0.2) L_{38}^{-1.8}$ sources per unit L_{38} per $10^{10} L_\odot$, where L_{38} is the X-ray luminosity in units of 10^{38} erg s $^{-1}$. This form for the luminosity distribution is in excellent agreement with that recently reported for the X-ray source population in M101 by Wang, Immler & Pietsch (1999) except that their normalisation (per $10^{10} L_\odot$) is a factor ~ 4 higher than our sample-averaged value[¶]. Almost certainly this represents a

[¶] We detect a total of 27 sources in M101 (= NGC 5457) - see Appendix A; Wang et al. (1999) exploit an ultra-deep co-addition

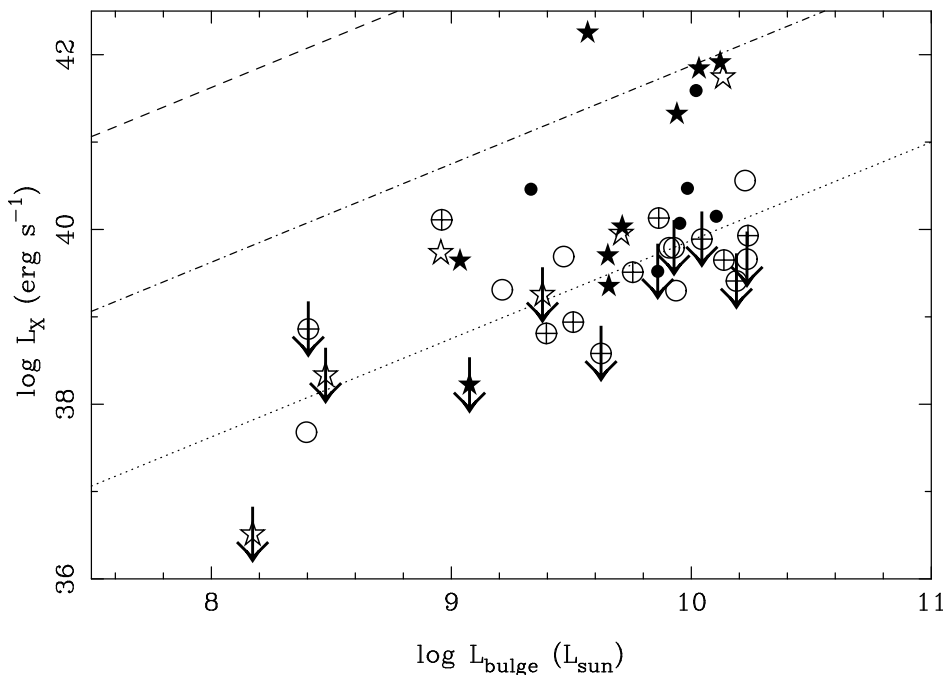


Figure 6. The X-ray luminosity of the Seyfert and LINERs in the XHFS sample plotted against the optical bulge luminosity of the host galaxy. The symbols for the various types of AGN are as per Figure 5. The diagonal lines represent the 10^{-2} (dashed), 10^{-4} (dot-dashed) and 10^{-6} (dotted) fractions of the Eddington luminosity (based on the assumptions described in the text).

real over-density of bright X-ray sources in M101 with respect to the norm for spiral galaxies and may be related to a number of factors such as the relatively low metallicity in the outer disk of M101 and the presence across the galaxy of numerous giant HII clouds and vigorous star-forming regions (Trinchieri, Fabbiano & Romaine 1990; Wang et al. 1999).

Integration of the luminosity distribution derived above for L_X in the range $10^{36} - 10^{40}$ erg s^{-1} , leads to an L_X/L_B ratio for the discrete X-ray source population in spiral galaxies of $1.1 \times 10^{39} \text{ erg s}^{-1} (10^{10} L_\odot)^{-1}$. In a recent paper Brown & Bregman (1998) have used *ROSAT* data to study the L_X versus L_B relation for a complete sample of early type galaxies. These authors estimate the contribution to the soft X-ray emission from stellar X-ray sources on the basis of X-ray spectral measurements for Cen A (the nearest non-dwarf elliptical galaxy). Specifically they use the results of Turner et al. (1997) who identify a hard spectral component in Cen A with stellar sources but attribute a soft component ($kT \approx 0.3$ keV) to emission from diffuse hot gas. The hard spectral component implies an L_X/L_B ratio for Cen A of $1.0 \times 10^{39} \text{ erg s}^{-1} (10^{10} L_\odot)^{-1}$, in excellent agreement with the value we derived above for spiral galaxies. (Note we have scaled up the hard X-ray luminosity for Cen A quoted by Brown & Bregman (1998) for the 0.5–2 keV band by a factor of 2.3 to account for our wider 0.1–2.4 keV bandpass).

of all the available HRI data and a detection threshold set at 3.5σ in deriving a list of 51 X-ray sources, about half of which are probably associated with M101.

The luminosity function defined above may also be integrated to give an estimate of the frequency of occurrence in spiral galaxies of “super-luminous” galactic X-ray sources. Here we define a super-luminous source (SLS) to be one with a luminosity above $L_X = 10^{38.3} \text{ erg s}^{-1}$, which is the Eddington limit for accretion onto a $1.4 M_\odot$ neutron star. We find that, on average, there are ~ 0.7 such sources per $10^{10} L_\odot$. The source catalogue in Appendix A actually lists 85 non-nuclear SLS, 28 of which have L_X in excess of $10^{39.0} \text{ erg s}^{-1}$.

The nature of the SLS population in nearby galaxies has been the subject of considerable debate following the discovery of many such objects in *EINSTEIN* and, more recently, *ROSAT* images (e.g. Fabbiano 1989; 1995; Read et al. 1997). Populations of galactic X-ray source which may generate X-ray luminosities in excess of $10^{38.3} \text{ erg s}^{-1}$ include XRBs powered by accretion onto a stellar mass ($M_{BH} < 10^2 M_\odot$) black hole and very young SNRs in which the supernova ejecta interact strongly with the circumstellar medium (e.g. Fabbiano, 1996 and references therein). Recently it has also been suggested that very luminous remnants observed in M101 may be the relics of “hypernovae”, that is to say local manifestations of gamma-ray burst activity (Wang 1999).

An important step when dealing with a point-like source which is apparently super-luminous is to consider whether it represents one discrete object or a complex of sources (for example, a dense grouping of high and/or low mass XRBs which individually would not be categorised as a SLS population). In this respect large amplitude variability provides a pointer towards the presence of either a single compact

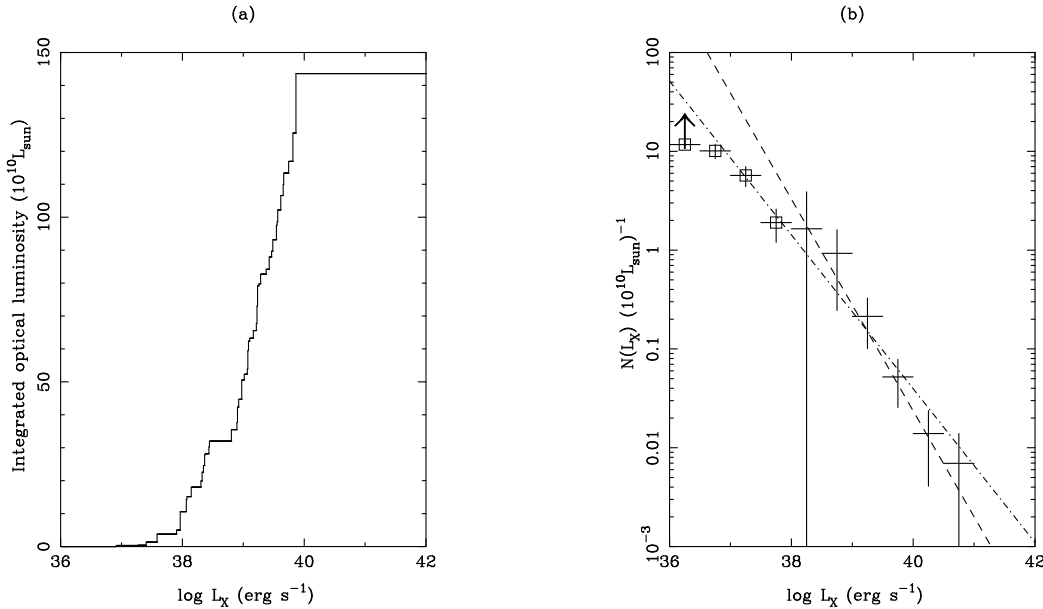


Figure 7. (a) The coverage correction used in calculating the luminosity distribution of the non-nuclear X-ray sources. (b) The luminosity distribution for non-nuclear sources per half decade bin in L_X normalised to $10^{10} L_{\odot}$ in L_B . This distribution is calculated for the set of 49 spiral galaxies (with $T = 0 - 6$) in the XHFS sample. The points (open squares) plotted below $L_X = 10^{38} \text{ erg s}^{-1}$ are for M 31 (Supper et al. 1997). Power-law fits both to the XHFS data alone and combined with M31 measurements are shown as the dashed and dashed-dotted lines respectively.

source or a grouping of no more than a few such objects. We have used the multiple HRI observations, where available, to identify those sources exhibiting significant (*i.e.* factor ≥ 2) variability (see Appendix A). It turns out that only 1 out of 19 of the non-nuclear SLS sources is flagged as variable, but unfortunately due to the limited temporal sampling it is difficult to draw any firm conclusions from this result.

In conclusion it seems likely that the non-nuclear SLS sources in the XHFS sample represent a heterogeneous mix of luminous stellar mass black hole XRBS, complexes of near-Eddington limited (or perhaps super-Eddington) high- and low-mass XRBS and a number of examples of recent supernovae and young SNRs. However, the detailed follow-up of individual sources is beyond the scope of the present paper.

6 SUMMARY

This paper utilises the substantial resources of both the *ROSAT* HRI public archive and the HFS sample to study the statistical properties of discrete X-ray sources in bright nearby galaxies. Our main findings may be summarised as follows:

- (i) Our XHFS catalogue lists 187 discrete X-ray sources detected within the optical extent of 83 nearby galaxies. The 45 sources which lie within $25''$ of the optical nucleus of the host galaxy are designated as “nuclear” X-ray sources with the remainder comprising our “non-nuclear” source sample.
- (ii) Contamination of the XHFS sample by background

and/or foreground objects is low. It amounts to less than 1 in 8 of the non-nuclear sample and is totally negligible in the nuclear sample.

(iii) The detection rate of nuclear X-ray sources and the average X-ray luminosity is substantially higher for those galaxies potentially hosting a low-luminosity AGN (Seyferts and LINERs) compared to the galaxies exhibiting only low-excitation emission spectra (the H II galaxies) or no emission lines.

(iv) The $L_X/L_{\text{H}\alpha}$ ratio of the putative AGN in the XHFS sample is in the same range as that observed for higher luminosity objects, such as QSOs, but extends two magnitudes fainter in luminosity than previously reported. Using the M_{BH} to L_{bulge} relation from Magorrian et al. (1998), we find that the low-luminosity AGN in the XHFS sample are radiating at severely sub-Eddington rates (*i.e.* $\sim 10^{-6} - 10^{-3}$ of the Eddington luminosity).

(v) The luminosity distribution of the non-nuclear sources in spiral galaxies of type SOa - Scd is $dN/dL_{38} = (1.0 \pm 0.2)L_{38}^{-1.8}$ sources per unit L_{38} per $10^{10} L_{\odot}$ in the $10^{36} - 10^{40} \text{ erg s}^{-1}$ range. This integrates to give a L_X/L_B ratio of $1.1 \times 10^{39} \text{ erg s}^{-1} (10^{10} L_{\odot})^{-1}$.

(vi) The median luminosity of the non-nuclear sources is ~ 10 times lower than that of nuclear sources. However, it is still in excess of the Eddington luminosity for a 1.4 solar mass neutron star ($\approx 10^{38.3} \text{ erg s}^{-1}$), implying a substantial population of super-luminous X-ray sources in nearby galaxies. Our estimate of the incidence such sources is ~ 0.7 per $10^{10} L_{\odot}$.

Although we discuss the possible nature of the super-luminous X-ray sources revealed in the XHFS survey in large numbers, we have not pursued the identification of individual sources, and indeed such a programme is greatly hampered by the limitations of the current X-ray data. This should change with the advent of the new generation of X-ray observatories, most particularly *XMM* and *CHANDRA*, whose combination of excellent spatial resolution, wide bandpass medium resolution spectroscopy and high throughput are ideally suited to detailed studies of the bright X-ray source populations in nearby galaxies.

ACKNOWLEDGMENTS

TPR gratefully acknowledges financial support from PPARC. The X-ray data used in this work were all obtained from the Leicester Database and Archive Service (LEDAS) at the Department of Physics & Astronomy, University of Leicester. The Digitised Sky Survey was produced at the Space Telescope Science Institute, under US government grant NAG W-2166 from the original National Geographic-Palomar Sky Survey plates. We are grateful to the anonymous referee for suggesting a number of improvements to this paper.

REFERENCES

- Allan D.J., 1995, Asterix user note 004, CCLRC/Rutherford Appleton Laboratories
- Brown B.A., Bregman J.N., 1998, *ApJL*, 495, 75
- Burstein D., Jones C., Forman W., Marston A.P., Marzke R.O., 1997, *ApJS*, 111, 163
- Colbert E.J.M., Mushotzky R.F., 1999, *ApJ*, 519, 89
- Dahlem M., Heckman T.M., Fabbiano, G., 1995, *ApJ*, 442, L49
- de Vaucouleurs G., de Vaucouleurs A., Corwin H.G., Jr., Buta R.J., Paturel G., Fouque R., 1991, *Third Reference Catalogue of Bright Galaxies*, Springer, New York
- Fabbiano G., 1989, *ARA&A*, 27, 87
- Fabbiano G., Kim D.-W., Trinchieri G., 1992, *ApJS*, 80, 645
- Fabbiano G., 1995, In 'X-ray Binaries', W.H.G. Lewin et al. eds., Cambridge University Press, Cambridge, 390
- Fabbiano G., 1996, In 'Roentgenstrahlung from the Universe', MPE report No. 263, H.U. Zimmermann, J.E. Tremper & H. Yorke eds., 347
- Fabbiano G., Juda J.Z., 1997, *ApJ*, 476, 666
- Fabian A.C., Rees M.J., 1995, *MNRAS*, 277, 55
- Feigelson E.D., Nelson P.I., 1985, *ApJ*, 293, 192
- George I.M., Turner T.J., Netzer H., Nandra K., Mushotzky R.F., Yaqoob T., 1998, *ApJS*, 114, 73
- Harris D.E., Silverman J.D., Hasinger G., Lehmann I., 1998, *A&AS*, 133, 431
- Hasinger G., Burg R., Giacconi R., Schmidt M., Trümper J., Zamorani G., 1993, *A&A*, 273, 1
- Ho L.C., 1999, *ApJ*, 516, 672
- Ho L.C., Filippenko A.V., Sargent W.L.W., 1995, *ApJS*, 98, 477
- Ho L.C., Filippenko A.V., Sargent W.L.W., 1997a, *ApJS*, 112, 315
- Ho L.C., Filippenko A.V., Sargent W.L.W., 1997b, *ApJS*, 112, 391
- Ho L.C., Filippenko A.V., Sargent W.L.W., 1997c, *ApJ*, 487, 568
- Ishisaki Y., Makashima K., Iyomoto N., Hayashida K., Inoue H., Mitsuda K., Tanaka Y., Ueno S., Kohmura Y., Mushotzky R.F., Petre R., Serlemitsos P.J., Terashima Y., 1996, *PASJ*, 48, 237
- Koratkar A., Deustra S.E., Heckman T., Filippenko A.V., Ho L.C., Rao M., 1995, *ApJ*, 440, 132
- Kormendy J., Richstone D., 1995, *ARA&A*, 33, 581
- Lawrence A., 1999, in Schmitt H.R., Kinney A.L., Ho L.C., eds, *Adv. in Sp. Res.*, Vol. 23, No. 5/6, 'The AGN/normal galaxy connection', pg. 1167, Oxford:Elsevier
- Lira P., Lawrence A., O'Brien P., Johnson R.A., Terlevich R., Bannister N., 1999, *MNRAS*, 305, 109
- Loewenstein M., Hayashida K., Toneri T., Davis D.S., 1998, *ApJ*, 497, 681
- Magorrian J., Tremaine S., Richstone D., Bender R., Bower G., Dressler A., Faber S.M., Gebhardt K., Green R., Grillmair C., Kormendy J., Lauer T., 1998, *AJ*, 115, 2285
- Narayan R., Yi I., 1995, *ApJ*, 452, 710
- Primini F.A., Forman W., Jones C., 1993, *ApJ*, 410, 615
- Ptak A., Yaqoob T., Serlemitsos P.J., Kuneida H., Terashima Y., 1996, *ApJ*, 459, 542
- Read A.M., Ponman T.J., Strickland D.K., 1997, *MNRAS*, 286, 626
- Roberts T.P., Warwick R.S., Ohashi T., 1999, *MNRAS*, 304, 52
- Salucci P., Ratnam C., Monaco P., Danese L., 1999, *MNRAS*, in press
- Siemiginowska A., Czerny B., Kostyunin V., 1996, *ApJ*, 458, 491
- Stark A., Gammie C.F., Wilson R.W., Bally J., Linke R.A., Heiles C., Hurwitz M., 1992, *ApJS*, 79, 77
- Supper R., Hasinger G., Pietsch W., Trümper J., Jain A., Magnier E.A., Lewin W.H.G., Van Paradijs J., 1997, *A&A*, 317, 328
- Trinchieri G., Fabbiano G., Romaine S. 1990, *ApJ*, 356, 110
- Turner T.J., George I.M., Nandra K., Mushotzky R.F., 1997, *ApJ*,

488, 164
Wandel A., 1999, ApJL, 519, 39
Wang Q.D., ApJL, 517, 27
Wang Q.D., Immler S., Pietsch W., 1999, ApJ, 523, 121
Whittle M., 1992, ApJS, 79, 49

APPENDIX A: CATALOGUE OF DETECTED X-RAY SOURCES

The complete, compressed catalogue of individual X-ray sources observed within the D₂₅ ellipse of the XHFS galaxies is presented in Table A1. All position and count rate data are determined by the PSS algorithm, and the nuclear separation is the observed distance between the HFS nuclear position and the X-ray source. Where there is more than one detection of a source, the data are combined with a weighting commensurate with the observation durations. The time-averaged count rates have been converted to flux as described in §2. Finally, the notes column shows an “N” if the source is a nuclear X-ray source, and a “v” if it is designated a variable source on the basis of its count rate varying by a factor ≥ 2 between detections in two separate observation epochs.

APPENDIX B: UPPER LIMITS ON NUCLEAR X-RAY LUMINOSITY

95% upper limits on the nuclear X-ray luminosities were derived for those nuclei without a detected nuclear X-ray source. The results are listed in Table B1. Where there are two or more observations of a source, the observation with the longest exposure was employed.

Table A1. Catalogue of the 187 discrete X-ray sources which comprise the XHFS sample.

Source designation	Observations	RA(2000)	dec(2000)	Count rate ($\times 10^{-3}$ count s $^{-1}$)	Nuclear offset ($''$)	log L $_X$ (erg s $^{-1}$)	Notes
IC 10 X-1	AB	00 ^h 20 ^m 29.7 ^s	59°16'48"	8.7 ± 0.4	57.5	38.41	
NGC 185 X-1		00 ^h 39 ^m 02.7 ^s	48°24'09"	1.7 ± 0.4	243.5	36.87	
NGC 205 X-1		00 ^h 39 ^m 52.5 ^s	41°45'17"	1.1 ± 0.3	405.4	36.59	
NGC 205 X-2		00 ^h 40 ^m 08.4 ^s	41°40'12"	1.2 ± 0.3	167.5	36.64	
NGC 221 X-1		00 ^h 42 ^m 35.6 ^s	40°48'32"	2.7 ± 0.6	224.7	36.99	
NGC 221 X-2		00 ^h 42 ^m 43.2 ^s	40°51'47"	13.4 ± 1.1	12.2	37.69	N
NGC 404 X-1		01 ^h 09 ^m 26.9 ^s	35°43'01"	1.2 ± 0.3	4.0	37.68	N
NGC 891 X-1		02 ^h 22 ^m 26.6 ^s	42°18'27"	0.6 ± 0.1	167.2	38.63	
NGC 891 X-2		02 ^h 22 ^m 30.8 ^s	42°19'07"	0.6 ± 0.1	110.6	38.60	
NGC 891 X-3		02 ^h 22 ^m 31.5 ^s	42°19'54"	4.8 ± 0.3	64.4	39.53	
NGC 891 X-4		02 ^h 22 ^m 31.6 ^s	42°20'19"	1.9 ± 0.2	43.6	39.12	
NGC 891 X-5		02 ^h 22 ^m 45.7 ^s	42°25'53"	1.6 ± 0.2	327.7	39.06	
IC 342 X-1		03 ^h 45 ^m 56.0 ^s	68°04'55"	8.2 ± 0.7	303.6	39.00	
IC 342 X-2		03 ^h 46 ^m 07.3 ^s	68°07'06"	1.9 ± 0.4	250.2	38.36	
IC 342 X-3		03 ^h 46 ^m 16.6 ^s	68°11'14"	2.7 ± 0.4	378.9	38.52	
IC 342 X-4		03 ^h 46 ^m 46.4 ^s	68°09'47"	4.9 ± 0.6	245.0	38.78	
IC 342 X-5		03 ^h 46 ^m 49.6 ^s	68°05'47"	7.4 ± 0.7	3.9	38.96	N
IC 342 X-6		03 ^h 46 ^m 58.5 ^s	68°06'18"	3.8 ± 0.5	61.5	38.67	
IC 342 X-7		03 ^h 48 ^m 07.6 ^s	68°04'54"	1.3 ± 0.3	439.6	38.19	
NGC 1569 X-1		04 ^h 30 ^m 48.7 ^s	64°50'47"	5.3 ± 0.8	10.3	38.22	N
NGC 1961 X-1		05 ^h 42 ^m 04.4 ^s	69°22'43"	1.6 ± 0.2	7.4	40.56	N
NGC 2276 X-1	AB	07 ^h 26 ^m 49.5 ^s	85°45'49"	1.5 ± 0.2	47.9	40.16	
NGC 2403 X-1		07 ^h 36 ^m 26.5 ^s	65°35'37"	13.1 ± 0.8	161.2	39.19	
NGC 2403 X-2		07 ^h 36 ^m 52.9 ^s	65°34'54"	1.0 ± 0.3	68.0	38.09	
NGC 2403 X-3		07 ^h 36 ^m 56.8 ^s	65°35'38"	4.0 ± 0.5	37.2	38.67	
NGC 2403 X-4		07 ^h 37 ^m 03.4 ^s	65°39'33"	3.6 ± 0.4	222.2	38.63	
NGC 2782 X-1		09 ^h 14 ^m 04.4 ^s	40°07'38"	1.7 ± 0.4	49.4	40.11	
NGC 2782 X-2		09 ^h 14 ^m 05.4 ^s	40°06'46"	7.3 ± 0.7	12.4	40.75	N
NGC 2903 X-1		09 ^h 32 ^m 05.6 ^s	21°32'32"	1.0 ± 0.3	169.4	38.39	
NGC 2903 X-2		09 ^h 32 ^m 09.9 ^s	21°31'01"	1.6 ± 0.4	65.1	38.60	
NGC 2903 X-3		09 ^h 32 ^m 10.4 ^s	21°30'05"	9.6 ± 1.0	9.1	39.38	N
NGC 2976 X-1	ABC	09 ^h 47 ^m 14.5 ^s	67°55'42"	2.3 ± 0.2	41.4	37.84	v
NGC 3031 X-1	F	09 ^h 54 ^m 51.9 ^s	69°02'48"	3.7 ± 0.5	251.6	37.69	
NGC 3031 X-2	ACDEFG	09 ^h 55 ^m 01.0 ^s	69°07'41"	1.3 ± 0.1	287.4	37.25	
NGC 3031 X-3	ABCDFG	09 ^h 55 ^m 03.0 ^s	68°56'15"	1.2 ± 0.1	504.0	37.21	v
NGC 3031 X-4	A	09 ^h 55 ^m 10.8 ^s	69°04'03"	4.5 ± 0.5	137.4	37.78	
NGC 3031 X-5	ABCDEFG	09 ^h 55 ^m 11.3 ^s	69°04'58"	1.8 ± 0.1	144.8	37.38	v
NGC 3031 X-6	F	09 ^h 55 ^m 13.2 ^s	69°08'25"	1.8 ± 0.4	287.3	37.37	
NGC 3031 X-7	ABCDEFG	09 ^h 55 ^m 23.1 ^s	69°05'07"	1.4 ± 0.1	94.4	37.26	
NGC 3031 X-8	ABCDEFG	09 ^h 55 ^m 25.3 ^s	69°09'56"	4.5 ± 0.2	355.0	37.77	
NGC 3031 X-9	BCDEFG	09 ^h 55 ^m 25.7 ^s	69°01'08"	12.5 ± 0.4	186.4	38.22	v
NGC 3031 X-10	F	09 ^h 55 ^m 27.2 ^s	69°02'50"	1.3 ± 0.4	90.2	37.24	
NGC 3031 X-11	ABCDEFG	09 ^h 55 ^m 34.0 ^s	69°00'28"	25.7 ± 0.5	217.9	38.53	
NGC 3031 X-12	C	09 ^h 55 ^m 34.1 ^s	69°02'42"	1.3 ± 0.4	84.9	37.24	
NGC 3031 X-13	ABCDEFG	09 ^h 55 ^m 34.2 ^s	69°03'50"	334.0 ± 1.6	19.6	39.64	N,v
NGC 3031 X-14	CF	09 ^h 55 ^m 38.5 ^s	69°02'40"	1.9 ± 0.3	86.6	37.41	
NGC 3031 X-15	BF	09 ^h 55 ^m 50.2 ^s	68°58'33"	1.1 ± 0.2	340.4	37.16	
NGC 3031 X-16	ABCDEFG	09 ^h 55 ^m 51.0 ^s	69°05'28"	2.8 ± 0.2	113.8	37.56	
NGC 3031 X-17	ABC	09 ^h 56 ^m 10.3 ^s	69°01'01"	1.4 ± 0.2	258.7	37.25	v
NGC 3031 X-18	ABCDG	09 ^h 56 ^m 15.4 ^s	68°57'18"	1.5 ± 0.1	458.3	37.29	v
NGC 3031 X-19	BD	09 ^h 56 ^m 37.7 ^s	69°00'25"	1.1 ± 0.2	396.0	37.18	
NGC 3031 X-20	BC	09 ^h 57 ^m 02.5 ^s	68°54'53"	1.2 ± 0.2	721.1	37.20	
NGC 3079 X-1	ABCDE	10 ^h 01 ^m 59.0 ^s	55°40'45"	2.6 ± 0.2	14.0	39.73	N,v
NGC 3147 X-1	ABC	10 ^h 16 ^m 54.4 ^s	73°24'00"	53.2 ± 0.9	3.7	41.74	N
NGC 3190 X-1		10 ^h 18 ^m 05.8 ^s	21°49'59"	2.1 ± 0.3	21.1	39.79	N
NGC 3226 X-1		10 ^h 23 ^m 27.3 ^s	19°53'54"	3.7 ± 0.4	8.0	40.07	N
NGC 3227 X-1		10 ^h 23 ^m 30.8 ^s	19°51'51"	84.6 ± 1.8	4.8	41.32	N
NGC 3310 X-1		10 ^h 38 ^m 46.1 ^s	53°30'11"	23.5 ± 0.9	47.9	40.62	
NGC 3310 X-2		10 ^h 38 ^m 49.8 ^s	53°29'33"	1.0 ± 0.2	40.6	39.25	
NGC 3377 X-1		10 ^h 47 ^m 41.7 ^s	13°58'26"	0.8 ± 0.2	47.5	38.53	
NGC 3377 X-2		10 ^h 47 ^m 42.7 ^s	13°59'07"	1.2 ± 0.3	3.9	38.68	N

Source designation	Observations	RA(2000)	dec(2000)	Count rate ($\times 10^{-3}$ count s $^{-1}$)	Nuclear offset (")	log L _X (erg s $^{-1}$)	Notes
NGC 3379 X-1		10 ^h 47 ^m 50.2 ^s	12°34'55"	5.0 ± 0.5	5.4	39.30	N
NGC 3395 X-1		10 ^h 49 ^m 50.3 ^s	32°59'07"	1.4 ± 0.3	26.6	39.75	
NGC 3628 X-1		11 ^h 20 ^m 15.7 ^s	13°35'23"	12.3 ± 1.0	31.9	39.62	
NGC 3628 X-2		11 ^h 20 ^m 37.3 ^s	13°34'38"	3.3 ± 0.6	296.1	39.04	
NGC 3998 X-1		11 ^h 57 ^m 50.4 ^s	55°28'31"	1.8 ± 0.5	78.3	39.63	
NGC 3998 X-2		11 ^h 57 ^m 56.4 ^s	55°27'10"	161.7 ± 3.6	17.4	41.59	N
NGC 4051 X-1		12 ^h 03 ^m 09.8 ^s	44°31'54"	1168.9 ± 10.9	12.9	42.25	N
NGC 4088 X-1		12 ^h 05 ^m 32.8 ^s	50°32'43"	2.5 ± 0.6	23.2	39.62	N
NGC 4150 X-1		12 ^h 10 ^m 35.0 ^s	30°23'56"	25.3 ± 1.7	24.1	40.11	N
NGC 4151 X-1	A	12 ^h 10 ^m 22.4 ^s	39°21'46"	0.5 ± 0.1	185.6	39.03	
NGC 4151 X-2	AB	12 ^h 10 ^m 22.8 ^s	39°23'12"	0.6 ± 0.1	124.7	39.15	
NGC 4151 X-3	AB	12 ^h 10 ^m 33.0 ^s	39°24'18"	293.0 ± 1.2	10.7	41.84	N
NGC 4203 X-1		12 ^h 15 ^m 05.3 ^s	33°11'49"	59.0 ± 1.6	15.7	40.46	N
NGC 4214 X-1		12 ^h 15 ^m 38.3 ^s	36°19'17"	2.7 ± 0.3	37.7	38.26	
NGC 4235 X-1		12 ^h 17 ^m 10.3 ^s	07°11'25"	122.1 ± 2.6	7.6	41.91	N
NGC 4258 X-1	B	12 ^h 18 ^m 44.6 ^s	47°17'21"	1.0 ± 0.3	147.9	38.40	
NGC 4258 X-2	AB	12 ^h 18 ^m 45.9 ^s	47°18'26"	1.3 ± 0.2	121.1	38.49	
NGC 4258 X-3	AB	12 ^h 18 ^m 45.8 ^s	47°24'18"	1.2 ± 0.2	376.7	38.46	
NGC 4258 X-4	AB	12 ^h 18 ^m 55.2 ^s	47°16'45"	1.4 ± 0.2	100.4	38.52	
NGC 4258 X-5	B	12 ^h 18 ^m 57.1 ^s	47°21'20"	1.2 ± 0.3	178.7	38.46	
NGC 4258 X-6	AB	12 ^h 18 ^m 58.1 ^s	47°18'03"	9.1 ± 0.5	18.7	39.35	N
NGC 4258 X-7	AB	12 ^h 18 ^m 58.3 ^s	47°16'01"	1.5 ± 0.2	140.1	38.57	
NGC 4258 X-8	AB	12 ^h 19 ^m 04.6 ^s	47°18'27"	2.4 ± 0.3	69.4	38.76	
NGC 4291 X-1	AB	12 ^h 20 ^m 18.2 ^s	75°22'09"	3.0 ± 0.3	6.8	40.22	N
NGC 4321 X-1		12 ^h 22 ^m 51.1 ^s	15°49'33"	0.9 ± 0.2	59.2	39.17	
NGC 4321 X-2		12 ^h 22 ^m 55.0 ^s	15°49'16"	8.2 ± 0.5	8.2	40.13	N
NGC 4321 X-3		12 ^h 22 ^m 58.6 ^s	15°49'07"	0.7 ± 0.2	52.6	39.09	
NGC 4321 X-4		12 ^h 22 ^m 58.9 ^s	15°47'49"	0.8 ± 0.2	109.0	39.14	
NGC 4388 X-1		12 ^h 25 ^m 47.3 ^s	12°39'38"	6.3 ± 0.9	5.1	40.03	N
NGC 4395 X-1		12 ^h 26 ^m 01.9 ^s	33°31'31"	16.8 ± 1.3	177.9	39.06	
NGC 4435 X-1		12 ^h 27 ^m 40.9 ^s	13°04'44"	1.9 ± 0.4	8.2	39.51	N
NGC 4438 X-1		12 ^h 27 ^m 46.0 ^s	13°00'26"	8.2 ± 0.7	9.4	40.15	N
NGC 4449 X-1	ABC	12 ^h 28 ^m 09.7 ^s	44°05'04"	6.4 ± 0.4	61.9	38.48	
NGC 4449 X-2	BC	12 ^h 28 ^m 10.5 ^s	44°05'51"	2.0 ± 0.3	40.0	37.97	
NGC 4449 X-3	ABC	12 ^h 28 ^m 11.3 ^s	44°03'33"	2.9 ± 0.3	134.8	38.14	v
NGC 4449 X-4	ABC	12 ^h 28 ^m 11.6 ^s	44°06'41"	5.5 ± 0.4	63.7	38.41	
NGC 4449 X-5	B	12 ^h 28 ^m 13.3 ^s	44°06'22"	5.3 ± 0.6	39.3	38.40	
NGC 4449 X-6	AB	12 ^h 28 ^m 15.0 ^s	44°05'42"	1.4 ± 0.3	10.0	37.80	N
NGC 4449 X-7	ABC	12 ^h 28 ^m 18.4 ^s	44°06'29"	3.3 ± 0.3	64.8	38.19	v
NGC 4485 X-1	AB	12 ^h 30 ^m 30.9 ^s	41°41'39"	2.8 ± 0.3	18.9	39.12	N
NGC 4490 X-1	AB	12 ^h 30 ^m 32.4 ^s	41°39'12"	3.4 ± 0.3	67.2	39.06	
NGC 4490 X-2	AB	12 ^h 30 ^m 36.7 ^s	41°38'34"	6.1 ± 0.4	13.9	39.31	N
NGC 4490 X-3	A	12 ^h 30 ^m 38.8 ^s	41°37'43"	1.4 ± 0.3	47.0	38.66	
NGC 4490 X-4	AB	12 ^h 30 ^m 43.6 ^s	41°38'14"	2.4 ± 0.3	81.9	38.91	
NGC 4559 X-1		12 ^h 35 ^m 52.0 ^s	27°56'01"	17.5 ± 0.6	123.7	39.94	
NGC 4559 X-2		12 ^h 35 ^m 56.5 ^s	27°55'26"	0.8 ± 0.2	131.7	38.62	
NGC 4559 X-3		12 ^h 35 ^m 56.7 ^s	27°59'23"	0.8 ± 0.2	108.1	38.61	
NGC 4559 X-4		12 ^h 35 ^m 58.9 ^s	27°57'40"	11.3 ± 0.5	13.1	39.75	N
NGC 4559 X-5		12 ^h 36 ^m 03.5 ^s	27°57'55"	0.9 ± 0.2	75.9	38.67	
NGC 4569 X-1		12 ^h 36 ^m 50.1 ^s	13°09'43"	5.1 ± 0.6	21.5	39.93	N
NGC 4631 X-1	AB	12 ^h 41 ^m 55.7 ^s	32°32'12"	5.2 ± 0.5	147.7	39.11	
NGC 4631 X-2	A	12 ^h 41 ^m 57.5 ^s	32°31'59"	2.0 ± 0.5	127.1	38.69	
NGC 4651 X-1		12 ^h 43 ^m 42.8 ^s	16°23'34"	1.3 ± 0.3	15.1	39.31	N
NGC 4656 X-1		12 ^h 43 ^m 41.4 ^s	32°04'55"	3.0 ± 0.4	379.5	38.91	
NGC 4736 X-1	A	12 ^h 50 ^m 44.5 ^s	41°04'49"	0.6 ± 0.1	183.4	37.73	
NGC 4736 X-2	A	12 ^h 50 ^m 47.8 ^s	41°05'03"	0.6 ± 0.1	152.0	37.77	
NGC 4736 X-3	A	12 ^h 50 ^m 52.8 ^s	41°02'47"	0.4 ± 0.1	272.1	37.62	
NGC 4736 X-4	AB	12 ^h 50 ^m 53.3 ^s	41°07'08"	50.5 ± 0.7	12.7	39.69	N
NGC 4736 X-5	B	12 ^h 51 ^m 00.0 ^s	41°11'00"	1.7 ± 0.3	231.4	38.23	
NGC 4826 X-1		12 ^h 56 ^m 44.0 ^s	21°40'59"	6.5 ± 1.0	9.6	38.81	N
NGC 5005 X-1		13 ^h 10 ^m 56.6 ^s	37°03'24"	13.0 ± 0.8	6.9	40.47	N

Source designation	Observations	RA(2000)	dec(2000)	Count rate ($\times 10^{-3}$ count s $^{-1}$)	Nuclear offset (")	log L _X (erg s $^{-1}$)	Notes
NGC 5055 X-1		13 ^h 15 ^m 18.3 ^s	42°03'57"	1.4 ± 0.4	373.6	38.59	
NGC 5055 X-2		13 ^h 15 ^m 19.8 ^s	42°02'55"	16.5 ± 1.3	340.8	39.65	
NGC 5055 X-3		13 ^h 15 ^m 30.5 ^s	42°03'07"	2.2 ± 0.5	229.4	38.78	
NGC 5055 X-4		13 ^h 15 ^m 41.0 ^s	42°01'42"	2.8 ± 0.6	98.1	38.88	
NGC 5055 X-5		13 ^h 15 ^m 47.0 ^s	42°01'52"	3.7 ± 0.7	31.3	39.01	
NGC 5055 X-6		13 ^h 15 ^m 47.1 ^s	42°00'16"	1.8 ± 0.5	96.8	38.70	
NGC 5055 X-7		13 ^h 15 ^m 49.9 ^s	42°01'38"	3.2 ± 0.7	9.9	38.94	N
NGC 5055 X-8		13 ^h 15 ^m 51.7 ^s	42°01'34"	2.1 ± 0.5	25.3	38.76	
NGC 5055 X-9		13 ^h 16 ^m 02.6 ^s	42°01'48"	1.6 ± 0.4	142.9	38.65	
NGC 5194 X-1		13 ^h 29 ^m 40.1 ^s	47°12'35"	2.6 ± 0.3	140.5	38.91	
NGC 5194 X-2		13 ^h 29 ^m 43.9 ^s	47°11'30"	1.4 ± 0.3	96.5	38.64	
NGC 5194 X-3		13 ^h 29 ^m 46.5 ^s	47°10'38"	1.4 ± 0.3	100.3	38.65	
NGC 5194 X-4		13 ^h 29 ^m 53.2 ^s	47°11'40"	28.4 ± 1.0	11.5	39.95	N
NGC 5194 X-5		13 ^h 29 ^m 54.4 ^s	47°14'33"	1.2 ± 0.2	161.7	38.57	
NGC 5194 X-6		13 ^h 29 ^m 59.6 ^s	47°15'48"	2.5 ± 0.4	245.6	38.91	
NGC 5194 X-7		13 ^h 30 ^m 01.6 ^s	47°13'40"	5.8 ± 0.5	138.2	39.27	
NGC 5194 X-8		13 ^h 30 ^m 06.9 ^s	47°08'30"	0.7 ± 0.2	245.6	38.33	
NGC 5194 X-9		13 ^h 30 ^m 08.1 ^s	47°11'01"	7.2 ± 0.5	160.5	39.36	
NGC 5195 X-1		13 ^h 30 ^m 06.8 ^s	47°15'39"	1.3 ± 0.2	80.7	38.77	
NGC 5204 X-1	AB	13 ^h 29 ^m 39.2 ^s	58°25'01"	30.3 ± 1.1	19.6	39.57	N
NGC 5273 X-1		13 ^h 42 ^m 08.3 ^s	35°39'09"	2.3 ± 0.5	16.7	39.70	N
NGC 5457 X-1	CD	14 ^h 02 ^m 03.9 ^s	54°18'26"	0.6 ± 0.1	642.2	37.93	
NGC 5457 X-2	ABCD	14 ^h 02 ^m 22.5 ^s	54°17'52"	0.8 ± 0.1	500.0	38.06	v
NGC 5457 X-3	ABCD	14 ^h 02 ^m 28.6 ^s	54°16'21"	1.8 ± 0.1	499.4	38.44	
NGC 5457 X-4	BCD	14 ^h 02 ^m 28.6 ^s	54°12'37"	1.3 ± 0.1	656.8	38.30	
NGC 5457 X-5	C	14 ^h 02 ^m 29.0 ^s	54°26'29"	0.6 ± 0.1	508.4	37.95	
NGC 5457 X-6	ABCD	14 ^h 02 ^m 30.3 ^s	54°21'15"	3.7 ± 0.1	389.1	38.74	
NGC 5457 X-7	C	14 ^h 02 ^m 34.8 ^s	54°21'11"	0.3 ± 0.1	349.0	37.61	
NGC 5457 X-8	B	14 ^h 02 ^m 47.2 ^s	54°26'53"	1.0 ± 0.2	415.7	38.17	
NGC 5457 X-9	CD	14 ^h 02 ^m 53.3 ^s	54°21'08"	0.6 ± 0.1	187.7	37.93	
NGC 5457 X-10	ABCD	14 ^h 03 ^m 04.4 ^s	54°27'32"	3.2 ± 0.1	388.8	38.68	v
NGC 5457 X-11	ACD	14 ^h 03 ^m 13.3 ^s	54°20'51"	0.9 ± 0.1	27.2	38.15	
NGC 5457 X-12	D	14 ^h 03 ^m 13.6 ^s	54°20'02"	0.5 ± 0.1	72.8	37.89	
NGC 5457 X-13	B	14 ^h 03 ^m 16.0 ^s	54°27'30"	0.7 ± 0.2	375.6	38.03	
NGC 5457 X-14	AB	14 ^h 03 ^m 20.4 ^s	54°17'15"	1.7 ± 0.2	244.3	38.41	
NGC 5457 X-15	CD	14 ^h 03 ^m 22.4 ^s	54°19'41"	0.8 ± 0.1	115.0	38.06	
NGC 5457 X-16	BC	14 ^h 03 ^m 24.0 ^s	54°19'41"	0.6 ± 0.1	123.7	37.99	
NGC 5457 X-17	B	14 ^h 03 ^m 31.4 ^s	54°21'55"	0.9 ± 0.2	151.1	38.14	
NGC 5457 X-18	D	14 ^h 03 ^m 32.9 ^s	54°20'58"	1.1 ± 0.2	159.5	38.23	
NGC 5457 X-19	BCD	14 ^h 03 ^m 36.5 ^s	54°19'21"	0.6 ± 0.1	221.3	37.95	
NGC 5457 X-20	D	14 ^h 03 ^m 41.8 ^s	54°19'02"	0.5 ± 0.1	271.2	37.91	
NGC 5457 X-21	D	14 ^h 03 ^m 51.2 ^s	54°24'09"	0.6 ± 0.1	362.9	37.93	
NGC 5457 X-22	BCD	14 ^h 03 ^m 54.6 ^s	54°21'55"	0.9 ± 0.1	350.3	38.12	
NGC 5457 X-23	D	14 ^h 04 ^m 00.4 ^s	54°09'09"	0.4 ± 0.1	828.4	37.75	
NGC 5457 X-24	ABCD	14 ^h 04 ^m 15.0 ^s	54°26'02"	4.7 ± 0.1	599.9	38.84	
NGC 5457 X-25	CD	14 ^h 04 ^m 17.5 ^s	54°16'10"	0.6 ± 0.1	627.7	37.92	
NGC 5457 X-26	ABCD	14 ^h 04 ^m 22.5 ^s	54°19'20"	1.1 ± 0.1	603.2	38.21	v
NGC 5457 X-27	CD	14 ^h 04 ^m 29.7 ^s	54°23'51"	0.7 ± 0.1	673.3	38.00	
NGC 5905 X-1		15 ^h 15 ^m 23.7 ^s	55°30'57"	1.0 ± 0.2	8.4	40.01	N
NGC 6217 X-1	ABCDE	16 ^h 32 ^m 40.6 ^s	78°11'49"	2.8 ± 0.2	4.2	40.02	N
NGC 6503 X-1		17 ^h 49 ^m 12.8 ^s	70°09'24"	1.5 ± 0.4	82.8	38.57	
NGC 6946 X-1	AB	20 ^h 34 ^m 26.5 ^s	60°09'06"	1.3 ± 0.2	189.4	38.63	
NGC 6946 X-2	A	20 ^h 34 ^m 35.0 ^s	60°10'29"	0.5 ± 0.1	141.1	38.22	
NGC 6946 X-3	AB	20 ^h 34 ^m 37.0 ^s	60°09'26"	2.7 ± 0.2	110.4	38.96	
NGC 6946 X-4	A	20 ^h 34 ^m 49.4 ^s	60°05'48"	0.7 ± 0.2	218.3	38.38	
NGC 6946 X-5	A	20 ^h 34 ^m 50.1 ^s	60°12'15"	0.6 ± 0.1	170.6	38.28	
NGC 6946 X-6	AB	20 ^h 34 ^m 53.1 ^s	60°09'07"	2.6 ± 0.2	20.9	38.95	N
NGC 6946 X-7	A	20 ^h 34 ^m 57.4 ^s	60°08'25"	0.7 ± 0.2	72.3	38.39	
NGC 6946 X-8	A	20 ^h 34 ^m 58.5 ^s	60°09'37"	0.6 ± 0.2	50.9	38.33	
NGC 6946 X-9	AB	20 ^h 35 ^m 00.9 ^s	60°09'03"	3.5 ± 0.2	71.2	39.07	
NGC 6946 X-10	AB	20 ^h 35 ^m 01.2 ^s	60°10'06"	0.8 ± 0.1	80.9	38.44	
NGC 6946 X-11	AB	20 ^h 35 ^m 01.4 ^s	60°11'27"	16.4 ± 0.5	141.4	39.75	
NGC 6946 X-12	A	20 ^h 35 ^m 12.9 ^s	60°07'26"	0.6 ± 0.1	223.7	38.31	
NGC 6946 X-13	A	20 ^h 35 ^m 19.4 ^s	60°10'53"	0.6 ± 0.1	378.3	38.29	
NGC 7331 X-1		22 ^h 37 ^m 04.4 ^s	34°24'51"	2.8 ± 0.4	18.0	39.65	N

Table B1. 95% upper limits on the nuclear X-ray luminosity for those galaxies with no detected nuclear source.

Galaxy	Count rate ($\times 10^{-3}$ count s $^{-1}$)	log L _X (erg s $^{-1}$)
IC 10	0.38	37.05
NGC 147	0.63	36.43
NGC 185	0.74	36.51
NGC 205	1.24	36.66
NGC 520	1.44	39.84
NGC 891	1.04	38.86
NGC 1058	0.36	38.33
NGC 1560	0.86	37.84
NGC 2276	1.72	40.23
NGC 2366	0.68	37.57
NGC 2403	0.30	37.55
NGC 2775	1.55	39.48
NGC 2976	0.70	37.32
NGC 3073	0.77	39.14
NGC 3185	0.68	39.25
NGC 3193	1.47	39.66
NGC 3294	1.76	39.83
NGC 3310	1.25	39.34
NGC 3384	1.45	38.76
NGC 3389	1.08	39.52
NGC 3395	0.74	39.49
NGC 3628	1.15	38.58
NGC 4214	1.15	37.89
NGC 4395	2.46	38.22
NGC 4470	1.17	39.80
NGC 4527	2.53	39.41
NGC 4631	1.30	38.51
NGC 4638	1.40	39.36
NGC 4647	1.60	39.42
NGC 4656	1.35	38.56
NGC 4772	2.24	39.52
NGC 5195	2.11	38.99
NGC 5354	1.43	39.89
NGC 5457	0.48	37.85
NGC 5775	0.66	39.47
NGC 5850	1.15	39.79
NGC 6503	2.96	38.86
NGC 6654	1.05	39.81